A THEORETICAL STUDY OF TYPE PI 2

GEOMAGNETIC MICROPULSATIONS

RECOMMENDED:

Chairman, Advisory Committee

Head, Space Physics and
Atmospheric Sciences Program

APPROVED:

Vice Chancellor for Research and Advanced Study

6 May 1983
Date

A THEORETICAL STUDY OF TYPE PI 2 GEOMAGNETIC MICROPULSATIONS

A

THESIS

Presented to the Faculty of the University of Alaska

in Partial Fulfillment of the Requirements

for the Degree of

MASTER OF SCIENCE

By

David U. Longenecker, A.B., M.A.

Fairbanks, Alaska

MAY 1983

ABSTRACT

Pi 2 pulsations are long period magnetic oscillations superimposed onto the geomagnetic field. They are usually associated with the onset of auroral substorms. To gain an understanding of the generation of Pi 2 pulsations, an instability mechanism and a transient response mechanism are studied. The instability mechanism results from a deceleration of magnetospheric convection in the plasma sheet while the transient response mechanism arises from an enhancement of magnetospheric convection in the plasma sheet. Both mechanisms are reviewed and a one-dimensional wave equation is solved numerically to model the transient response mechanism. The numerical computations indicate that a rapid enhancement of the magnetospheric convection will launch Alfven waves which will produce an oscillating current in the ionosphere. Model results for the transient response mechanism indicate that the oscillating current can produce Pi 2 pulsations with periods that compare favorably with ground based measurements.

WHITE RABBIT

One pill makes you larger
And one pill makes you small
And the ones that mother gives you don't do anything at all
Go ask Alice, when she's ten feet tall
And if you go chasing rabbits and you know your going to fall
Tell them a hookah smoking caterpillar has given you the cord
Poor Alice, when she was just small
When the men on the chessboard get up and tell you where to go
And you've just had some kind of mushroom and your mind is moving low
Go ask Alice, I think she'll know
When logic and proportion have fallen sloppy dead
And the white is talking backwards
And the red queen's on her head
Remember what the doormouse said
Feed your head
Feed your head

-Grace Slick

TABLE OF CONTENTS

LIST OF FIGURES

LIST OF TABLES

ACKNOWLEDGEMENTS

I would like to thank Joe Enzweiler for drafting the figures, and John Olson for carefully reading the manuscript. Thanks are also due to all students, staff and faculty who helped me during my stay at the University of Alaska.

I INTRODUCTION

1.1 Introduction

Geomagnetic pulsations are variations of the earth's magnetic field with periods ranging from a few seconds to tens of minutes. Unlike the origin of the main magnetic field, which is internal to the earth, the pulsations are due to external sources.

The earth's magnetic field is rather weak compared to the magnetic field of magnets which are commonly found in the home or scientific laboratory. At the geomagnetic poles the magnetic field has a strength of about .62 Gauss. Geomagnetic pulsation amplitudes are about 10^{-5} times weaker. Usually the unit of gamma is used to designate magnetic fields of this strength. One gamma is 10^{-5} gauss.

In 1600 William Gilbert published the results of his studies on the characteristics of the magnetic field produced by a spherical piece of naturally magnetic material. He noticed that the inclination of the sphere's magnetic field to its surface was similar to the inclination of the earth's magnetic field to its surface. He concluded that the earth is essentially a magnetized sphere with its magnetic field being produced from within. Later, in 1839, Gauss' spherical harmonic analysis of a magnetized sphere showed that it is an excellent first approximation to th earth's magnetic field.

In 1741 Celsius noticed the association between fluctuations of the

earth's magnetic field and auroral displays. This study was done in association with Graham of London. Stewart (1861) reported on the magnetic disturbances of 1859. Since that time the study of geomagnetic pulsations has gone under the names of geomagnetic oscillations, fluctuations, micropulsations, pulsations, hydromagnetic emissions and others.

Angenheister (1912) was the first to report on a characteristic pulsation which is seen at the onset of geomagnetic bays. Since that time these pulsations have been studied under names such as night time pulsations and polar sudden commencement. In 1957 the Tenth Committee of IAGA named these pulsations pt, for pulsation train. Since 1964 (Jacobs et al., 1964) the IAGA designation for these pulsations has been Pi 2. These pulsations are defined as "long period pulsations which occur essentially at the beginning part of bays", (Saito, 1969). The classification scheme for all pulsations is given in Table (1.1).

Pi 2 pulsations are defined as the long period pulsations of the earth's magnetic field which are associated with auroral substorms. The period of these pulsations ranges from 40 to 150 seconds. The duration is from a few minutes up to about one-half hour. Mid-latitude Pi 2 pulsations are generally in the 100-130 second period range, and in the lower latitudes such as Japan, the period ranges from 32 to 65 seconds (Rostoker, 1967).

The amplitudes are greatest in the auroral zones. The longitudinal extent of Pi 2 pulsations is as much as 100^{o}, but the maximum amplitude is near local midnight.

Table (1.1). Classification of geomagnetic pulsations decided by IAGA at the 1963 Berkeley Meeting

Type		Period range (sec)
Continuous pulsations	Pc 1	0.2- 5
	Pc 2	5- 10
	Pc 3	10- 45
	Pc 4	45-150
	Pc 5	150-600
Irregular pulsations	Pi 1	1- 40
	Pi 2	40-150

Other irregular pulsations are associated with Pi 2 pulsations. Pi 1 pulsations are high frequency riders seen with Pi 2 pulsations at the onset of auroral substorms. The period range of Pi 1 pulsations is from 1 to 40 seconds. The duration of Pi 1 pulsations is usually shorter than the duration of Pi 2 pulsations. Another associated pulsation is the Pi C pulsation (Heacock, 1967). This is a continuous nonimpulsive pulsation seen in the night-morning sector.

The purpose of this thesis is to gain an understanding of origin and the characteristics of Pi 2 pulsations. For this purpose, the remainder of this chapter will be devoted to a review of observations and theories of Pi 2 pulsations.

1.2 Observations

Pi 2 pulsations are associated with the beginning of geomagnetic bays. A geomagnetic bay is characterized by a large decrease or increase in the horizonal component of the geomagnetic field. A geomagnetic bay signals the onset of a substorm. A good example of Pi 2 pulsations at the onset of a geomagnetic bay is given by Fig. (1.1). The top trace represents the variation of the horizonal component of the earth's magnetic field. The arrow, which points downward, indicates that a decrease in the H-component is represented by a rising of the trace. The ripples in the trace are the Pi 2 pulsations. The amplitude of the pulsations is on the order of a few gammas.

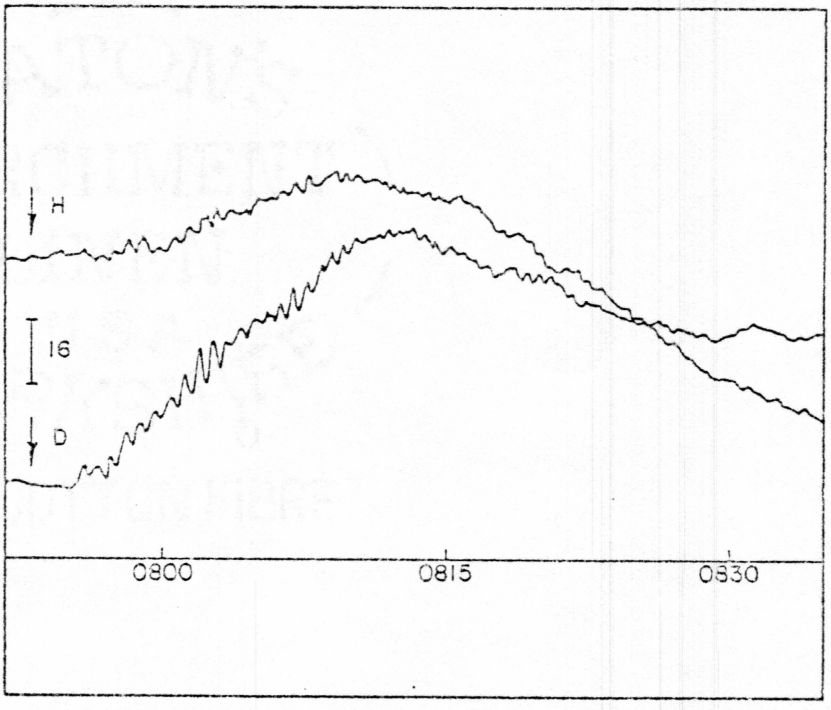

Fig. (1.1) An example of the H and D components of a geomagnetic bay showing the superposition of Pi 2 pulsations.

The geomagnetic bays are associated with large currents in the auroral ionosphere. The current flows in the westward direction in the evening hours and is known as the auroral electrojet. And, although the amplitude of Pi 2 pulsations is greatest in the auroral region, the amplitude is not necessarily proportional to the size of the associated bay (Saito, 1969).

Fig. (1.2) shows the magnetic field components for the period 5:00-8:00 UT for November 23, 1971, for the University of Alberta magnetometer chain (taken form Olson and Rostoker, 1977). The stations are arranged from north to south in western Canada. The names and locations are given in Table (1.2). A substorm onset takes place at about 6:45 UT. The component of the earth's magnetic field which is perpendicular to the surface is called the Z-component. Analysis of the Z-component gives an indication of the location of the auroral electrojet. A horizonal current flowing directly overhead will not have a verticle magnetic field component. The transition between positive Z-component and negative Z-component therefore indicates the location of the auroral electrojet. For the onset of this event the change in the Z-component appears between stations MENK and MCMU. Fig. (1.3) is an enlargement of the H-component plot of Fig. (1.2). The H-traces for SMIT, FTCH, and MCMU all indicate the large negative bay as well as the presence of Pi 2 pulsations. The Pi 2 pulsations are the upward excursions superimposed on the bay disturbance. The pulsations recorded at MCMU appear to have a greater amplitude than those at FTCH, and the pulsations at FTCH have a greater amplitude than those recorded at

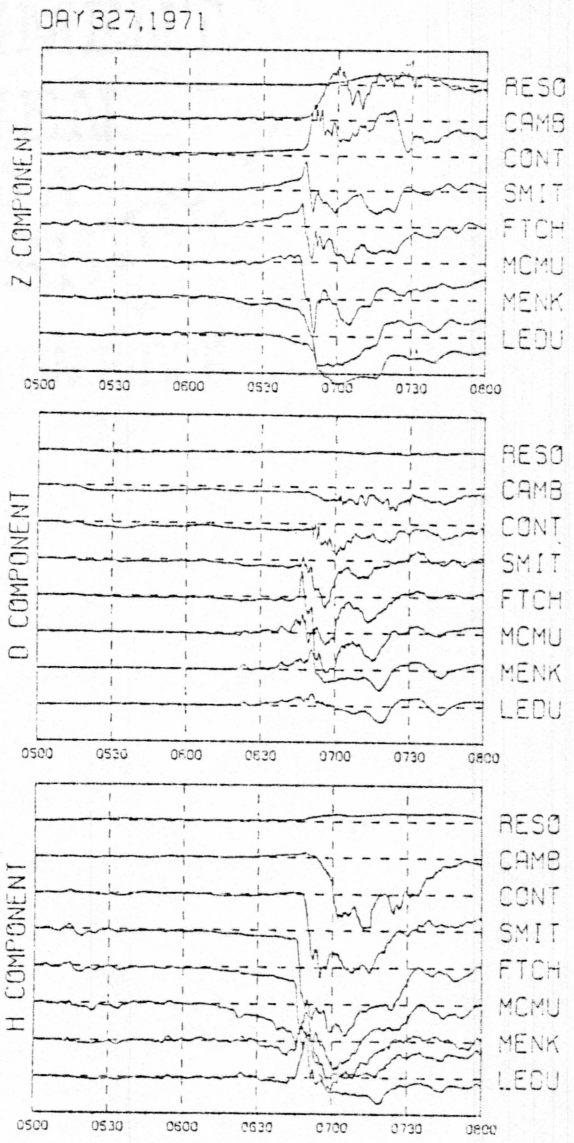

Fig. (1.2) The Z, D, and H components for the period 5:00-8:00 UT for November 23, 1971 as recorded by the University of Alberta magnetometer chain.

Table (1.2). Magnetometer Station Locations
University of Alberta

Station	Mnemonic	Centered dipole Lat.	Long.	L
Resolute Bay	RESO	83.0	289.4	71.4
Cambridge Bay	CAMB	76.8	296.6	19.5
Contwoyto Lake	CONT	72.6	295.8	11.3
Fort Reliance	RELI	70.3	300.1	8.9
Fort Smith	SMIT	67.3	300.0	6.8
Fort Chipewyan	FTCH	66.3	302.1	6.2
Fort McMurray	MCMU	64.2	303.5	5.4
Meanook	MENK	61.9	300.8	4.5
Leduc	LEDU	60.6	302.9	4.2
Calgary	CALG	58.4	302.9	3.7

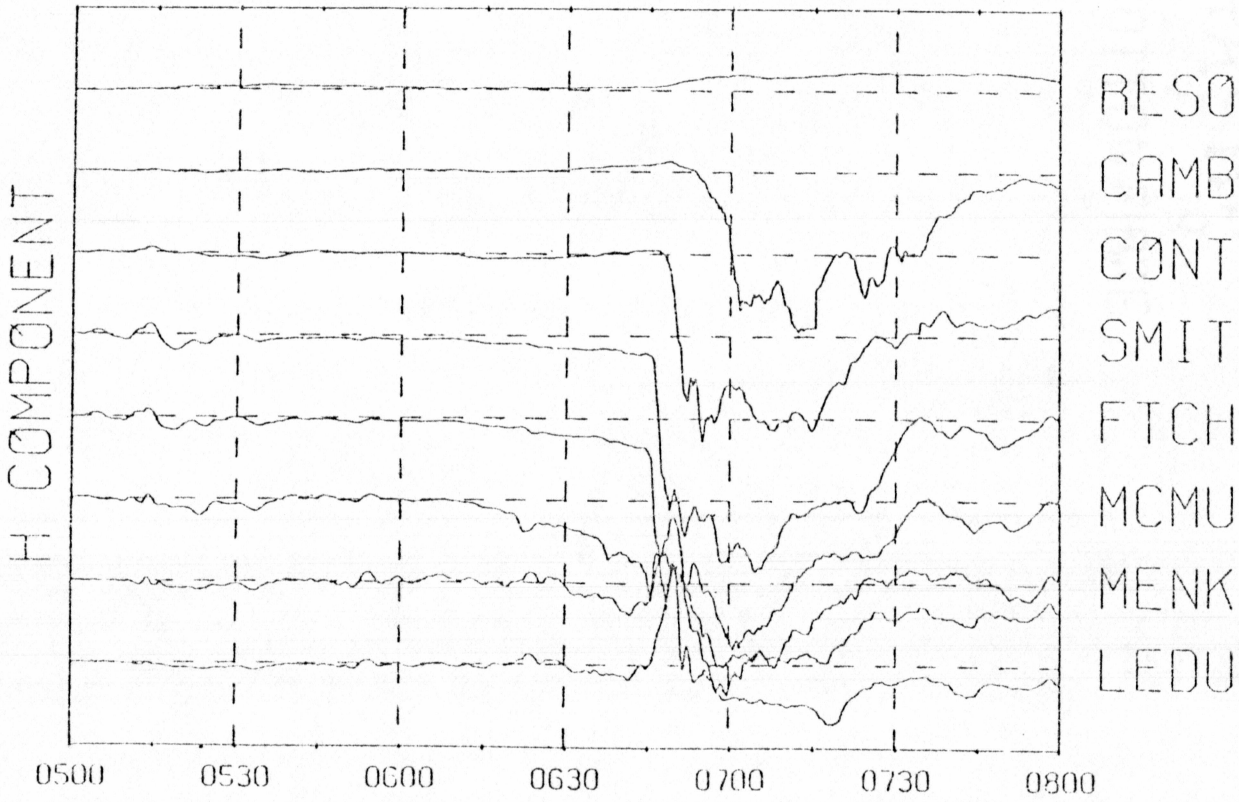

Fig. (1.3) H component for the same period as in Fig. (1.2).

SMIT. The general trend is for the amplitude to decrease as the distance of the observer from the auroral electrojet increases. Fig. (1.4) is filtered data for the same event. The low frequency geomagnetic bay has been removed from the data. After the geomagnetic bay has been removed, only the magnetic field due to the pulsations remains. The pulsation amplitude is the largest at MCMU and decreases steadily at the stations both north and south of MCMU.

Another feature of Pi 2 pulsations is their polarization. A recent paper (Pashin, et al., 1982) presents the latest data on polarization and evidence for a possible source of Pi 2 pulsations. The data for the paper (Pashin, et al., 1982) was obtained from the Scandinavian Magnetometer Array, SMA. The SMA is a group of magnetometer stations arranged in a large rectangle in northern Norway, Finland, Sweden and the adjoining area of the Soviet Union. The spacing between the stations is roughly uniform. Because the array is two-dimensional, information on the location of auroral phenomena can be determined better than by a one-dimensional chain of stations. In particular, the relationship of the polarization of Pi 2 pulsations and the westward auroral eletrojet can be determined. Fig. (1.5) shows the location of some of the stations of the SMA. Each station is indicated by a dot. The arrow around each dot indicates the sense of the rotation of the horizonal magnetic disturbance vector, i.e., the Pi 2 pulsation. A station with two arrows indicates an ambiguity in the polarization. The heavy lines indicate the location of the intense visual aurora. The location of the auroral electrojet and the intense visual aurora are

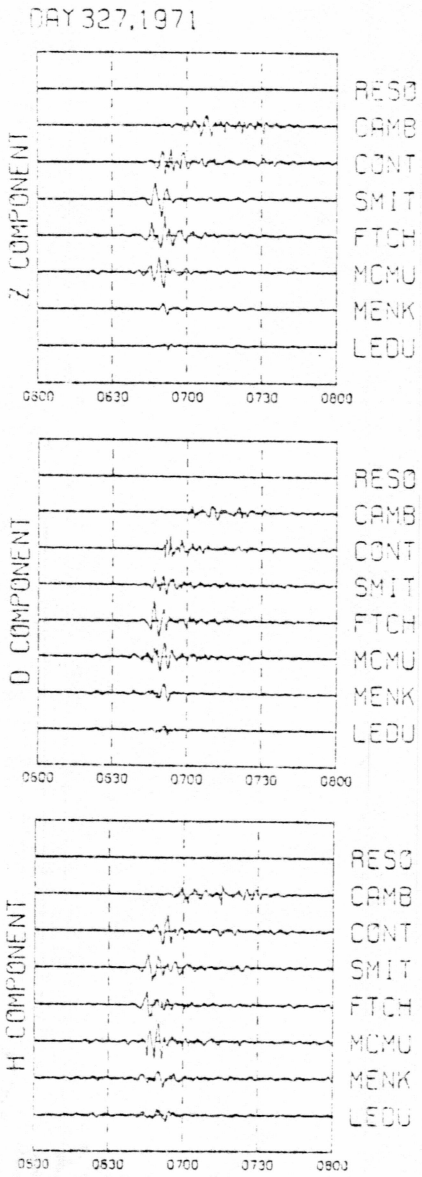

Fig. (1.4) Filtered data for the event of Fig. (1.2). The filter removes the geomagnetic bay component of the magnetic field.

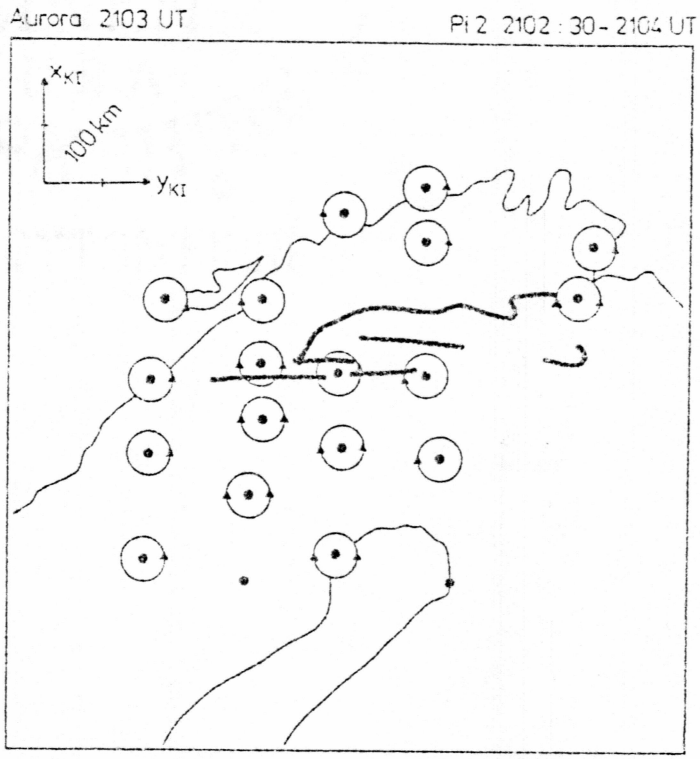

Fig. (1.5) The Scandinavian Magnetometer Array. The stations are represented by dots. The arrows around the stations indicate the sense of the polarization. The heavy line indicates the location of the bright aurora.

correlated. The north-south columns are refered to as profiles, the first profile being on the left, which is in the west. In the fourth profile the polarization of the Pi 2 pulsations change from clockwise south of the aurora to counter-clockwise north of the aurora. Changes in the polarization in the second and third profiles are not clear due to the difficulty of determining the polarization at the individual stations. The authors attribute this to the rather rapid movement of westward edge of the auroral electojet.

From the data on the polarization of the Pi 2 pulsations, the authors conclude that upward field-aligned currents in the vicinity of the westward edge of the auroral electrojet play an important role in generating Pi 2 pulsations. Fig. (1.6) shows two possible scenarios for producing two polarization patterns. The circles and the ellipse with the dot in the center indicates the location and shape of the upward field-aligned current for two distinct times. The dashed and solid lines point in the direction of the magnetic field which is produced by the current. The solid line is for the earlier time and the dashed line for the later time. As the current moves in the westward (to the left) direction, the magnetic field vector will rotate from the position of the solid line to the position of the dashed line. The polarization sense is given at the left. The top panel would produce a polarization situation like that of profile four of Fig. (1.5). In the lower panel, the upward field-aligned current begins as in the top panel, a circular distribution. As the current moves westward it may change from a circle to an ellipse, depending on ionospheric conditions. In this case the

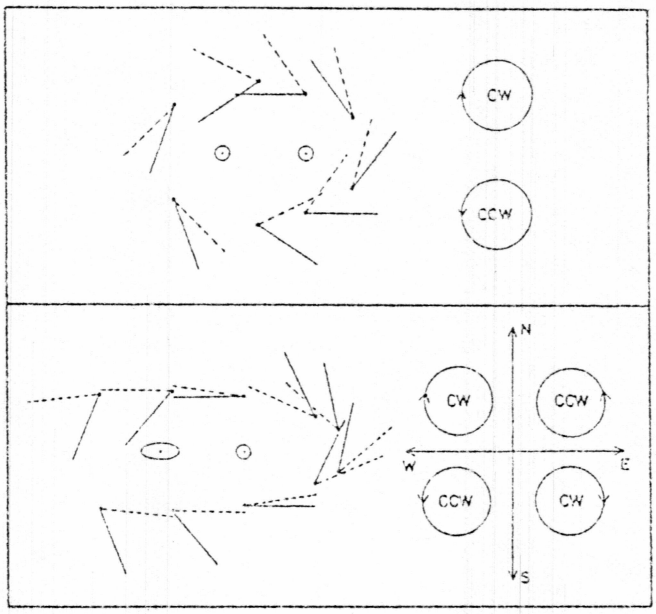

Fig. (1.6) Two cases of current distributions producing different polarization features. Top panel: A circular current moves from the right encircled dot to the left encircled dot. Bottom panel: A circular current moves to the left and as it does it changes to an elliptical current. The magnetic field direction is represented by solid and dashed lines for earlier and later times, respectively. The polarization is shown schematically at the left.

polarization pattern will develop into quadrants. The sense of the polarization is given at the right. A limitation on these two polarization schemes is that neither would be able to produce a 360° degree rotation of the polarization vector.

Satellite observations of Pi 2 pulsations have been made in recent years. Lin and Cahill (1975) describe the occurrence of Pi 2 pulsations in the magnetosphere as recorded by the Explorer 45 satellite. Measurements were made when the satellite was close to its apogee, near the equator at about 5 R_E from the earth. In the three month period they examined, thirteen substorms were identified when the satellite was near apogee. Of the thirteen substorms, pulsations were recorded in twelve of them. For seven of these twelve events, pulsations were recorded at several high latitude ground stations and were identified as Pi 2 pulsations. The period of the pulsations at the satellite differed from the period measured at the ground. For two events the range of periods on the ground was within the range of the periods at the satellite. For the other five events, the satellite periods were either higher or lower than the ground observed periods. Due to the varying nature of the periods recorded at the satellite and the ground, specific conclusions about the relationship between satellite and ground observed pulsation periods were not made. However, the authors did conclude that the pulsations in the magnetosphere do accompany substorm onsets.

This completes the review of observational work. In the next section, recent theoretical work will be reviewed.

1.3 Theories

The purpose of this section is to present a summary of theoretical work on Pi 2 pulsations. The first subsection will deal with possible instability mechanisms. In the second subsection transient response mechanisms are reviewed.

1.3.1 Instability Mechanisms

Pi 2 pulsations can be considered MHD waves which are generated by instability mechanisms in the plasma sheet. After being generated, the MHD waves propagate and can be detected by ground-based and satellite-borne instruments. While travelling from their source to the observation point, the characteristics of the waves can be modified. This then makes identifying the exact source and means of production difficult. Therefore, several instability mechanisms which appeared in the literature recently are presented here as possible sources of Pi pulsations.

The first is the drift instability described by Coroniti and Kennel (1970). In this paper the drift instability Alfven wave is considered. It is driven by an electron thermal gradient at the inner edge of the plasma sheet. The instability is localized to the radius of the region of maximum electron temperature gradient with wavelengths perpendicular to the magnetic field with a size of about the ion cyclotron radius. The wavelengths parallel to the magnetic field are

about the same size as the length of the field line. The fastest growing mode has a period of about ten seconds, according to the theory, which is comparable to the 5 to 15 second pulsation seen at the advent of a substorm. Note, however, that this period is below the Pi 2 period range which begins at 40 seconds. The authors used kinetic theory to derive the dispersion relationship under the following assumptions: (1) straight magnetic field configuration, (2) neglected ionospheric attenuation and coupling, and (3) considered only a small magnetic inhomogenity. The applicability of this mechanism might be limited to Pi 1 pulsations, however, since the generation of Pi 1 and Pi 2 pulsations appear to be related, it is included here.

Chang and Lanzerotti (1975) analyzed the instability of magnetoacoustic waves driven by a neutrally-charged particle beam in a plasma. They suggest that this instability can be generated in the near earth plasma sheet during a substorm onset. They also suggest that MHD waves seen at the substorm onset may be attributed to the coupling of magnetoacoustic waves and shear Alfven waves. They consider two cases. The first case pertains to the generation of slow magnetoacoustic waves. For this case the phase velocity of the magnetoacoustic wave in the beam reference frame must be much smaller than the mean thermal velocity of the electrons in the beam and the phase velocity must be much greater than the mean thermal velocity of the ions. The resultant growth rate is found to be independent of the ratio of the beam electron temperature to the plasma electron temperature. In the second case the phase velocity of the

magnetoacoustic wave in the beam reference frame is much greater than the mean thermal velocity of the electrons. For this case the instability criterion can be satisfied for waves in the Pi 2 frequency range. This model excludes flow due to convection.

Kan and Heacock (1976) presented a model which can produce Pi C type pulsations. Pi C type pulsations are pulsations which occur in the night-morning hours and are continuous in nature (Heacock 1967). This model relies on an enhanced pressure anisotropy resulting from enhanced field-aligned plasma flow along the plasma sheet. This activates the garden hose instability and produces the waves. The pressure anisotropy is due to the field-aligned streaming plasma and magnetic mirroring. The estimated length of the source region for the Pi C pulsations is compatible to the source length of $18R_E$ suggested by Nishida and Hones (1974).

The last instability mechanism to be considered here is the one due to Kan et al. (1982a). In this model the they propose that Alfven waves can be generated in the magnetosphere by deceleration of magnetospheric convection due to the dynamo process in the magnetospheric-ionspheric coupling. It is a one-dimensional model in which the magnetic field lines are treated as equipotentials. The results are derived using the local approximation of MHD theory. For moderately disturbed conditions unstable Alfven waves are produced if the convection speed exceeds 150 km/sec in the near-earth (10 to 20 R_E) plasma sheet (Hones et al., 1976). The characteristics of this mechanism can be summerized in four points: (1) the growth rate is proportional to the Pedersen conductivity

and the square of the convection speed in the region along the field lines connecting the northern and southern auroral ionospheres, (2) the growth rate of the Alfven packets is independent of the wave number (3) the growth rate can turn into a damping rate if the growth rate threshold is not met, (4) Alfven waves are guided along field lines and are unaffected by the instability.

This concludes the review of the instability mechanisms which could be responsible for the generation of Pi 2 pulsations. In the next subsection transient mechanisms will be reviewed.

1.3.2 Transient Response Mechanisms

The fundamental difference between instability produced pulsations and transient produced pulsations is that the instablity is a continuous source whereas the transient is an impulsive energy source. After being pulsed by a large transient, such as a change in the magnetospheric configuration or by a change in the magnetospheric convection, a wave can be produced which travels back and forth from the magnetosphere to the ionosphere. Ionospheric currents can be affected and produce pulsations of the magnetic field. In this subsection the transient response mechanism are reviewed.

Stuart (1974) presented a mechanism in which the Pi 2 pulsations could be produced on auroral field lines. This mechanism is capable of producing the secondary enhancements of the Pi 2 pulsation amplitudes which are seen in the mid-latitudes. The secondary enhancement comes

about by the constructive interference of waves traveling along field lines from the equatorial plane to the ionosphere and from waves travelling across field lines to the ionosphere from the equatorial equator.

Other authors indicated that Pi 2 pulsations could be generated in the ionosphere. Maltsev et al. (1974) considered the generation of Pi 2 pulsations in the ionosphere due to a sudden decrease in the ionospheric electric field. The impulse produces pulsations which then travel along the geomagnetic field lines and are reflected from the opposite ionospheres. They found that the resonance periods, i.e. the time it takes an impulse to travel from one ionosphere to the other ionosphere and return, to depend on the ionospheric conductivities.

Maltsev et al. (1977) considered a three-dimensional current system over a strip of enhanced conductivity to model currents over the auroral ionosphere. The strip of enhanced conductivity represents the auroral region. This model produced stationary Alfven waves which propagated along the geomagnetic field lines. The Alfven waves correspond to an appearance of field-aligned currents over an auroral arc. They found that two sheets of field-aligned currents were produced.

Heacock and Chao (1980) found that substorms with sharp onsets are preceded by Pi activity in the polar cap. They believe that anti-solar convection of the plasma over the polar cap causes the pulsations. The Pi pulsations appear to be caused by three-dimensional current loops which are driven by the magnetospheric electric field at the time of enhanced magnetospheric convection.

Mallinckrodt and Carlson (1978) showed that shear mode Alfven waves can be produced along a flux tube. The source location is arbitrary, however its location effects the resulting fields and currents. Comparison of data demonstrated that different results are expected for magnetospheric or ionospheric sources. The magnetospheric source predicts much better the ionospheric sheets currents which are observed.

Another feature of Pi 2 pulsations is their absorption in the ionosphere. Newton et al. (1978) showed that a significant sink of geomagnetic energy exists in the ionosphere. This is due to Joule dissipation. They investigated the dissipation of waves by computing the ionospheric damping in a model magnetic field. The boundary conditions at the ionosphere relates the electric and magnetic fields. The damping rates were found to be strongly dependent on the ionospheric conductivity. For a typical nighttime conductivity of about 10^{11} e.s.u. the waves were damped away in about four periods, which is consistant with observations.

This concludes the review of transient response mechanisms.

1.4 Summary

We have seen that Pi 2 pulsations are associated with Geomagnetic bays. The amplitude of the pulsations is the greatest in the auroral region and appears to associated with the auroral electrojet. Recent studies have shown that the polarization of the Pi 2 pulsations is

related to the position of the westward edge of the westward travelling auroral electrojet. The polarization sense seems to be dependent on the upward field-aligned currents.

The are two main types of generation mechanisms for Pi 2 pulsations. They are the instability mechanisms and the transient response mechanisms. In the first category we have reviewed instabilities created by electron thermal gradients, neutral beam-plasma in

II GENERATION OF PI PULSATIONS DUE TO DECELERATION OF MAGNETOSPHERIC CONVECTION

2.1 Introduction

The magneosphere-ionosphere coupling system can be described as a dynamo system in which the ionospheric load is connected to the magnetospheric dynamo by means of field-aligned currents (Rostoker and Bostrom, 1976; Sonnerup, 1980; Kan and Lee, 1980). A schematic diagram of this system is given in Fig. (2.1). The magnetospheric dynamo region is the inner or earth ward edge of the plasma sheet. The electric currents pictured are aligned with the magnetic field and are called field-aligned currents. The current flows along the magnetic field lines into the polar ionospheres. We assume that the ionospheric electric field is in the northward direction in the northern hemisphere and southward in the southern hemisphere. In the ionospheres, the currents flow poleward in the direction of the ionospheric electric fields. The conductivity of the ionospheres is not finite and thus acts as a load on this circuit. The conductivity as measured in the direction of an electric field is known as the Pedersen conductivity. In the case of the ionospheres, the current and electric field are parallel, and therefore, the conductivity is refered to as the Pedersen conductivity. The ionospheric load, which is due to the finite Pedersen conductivity, causes the plasma flow in the dynamo to decrease. This

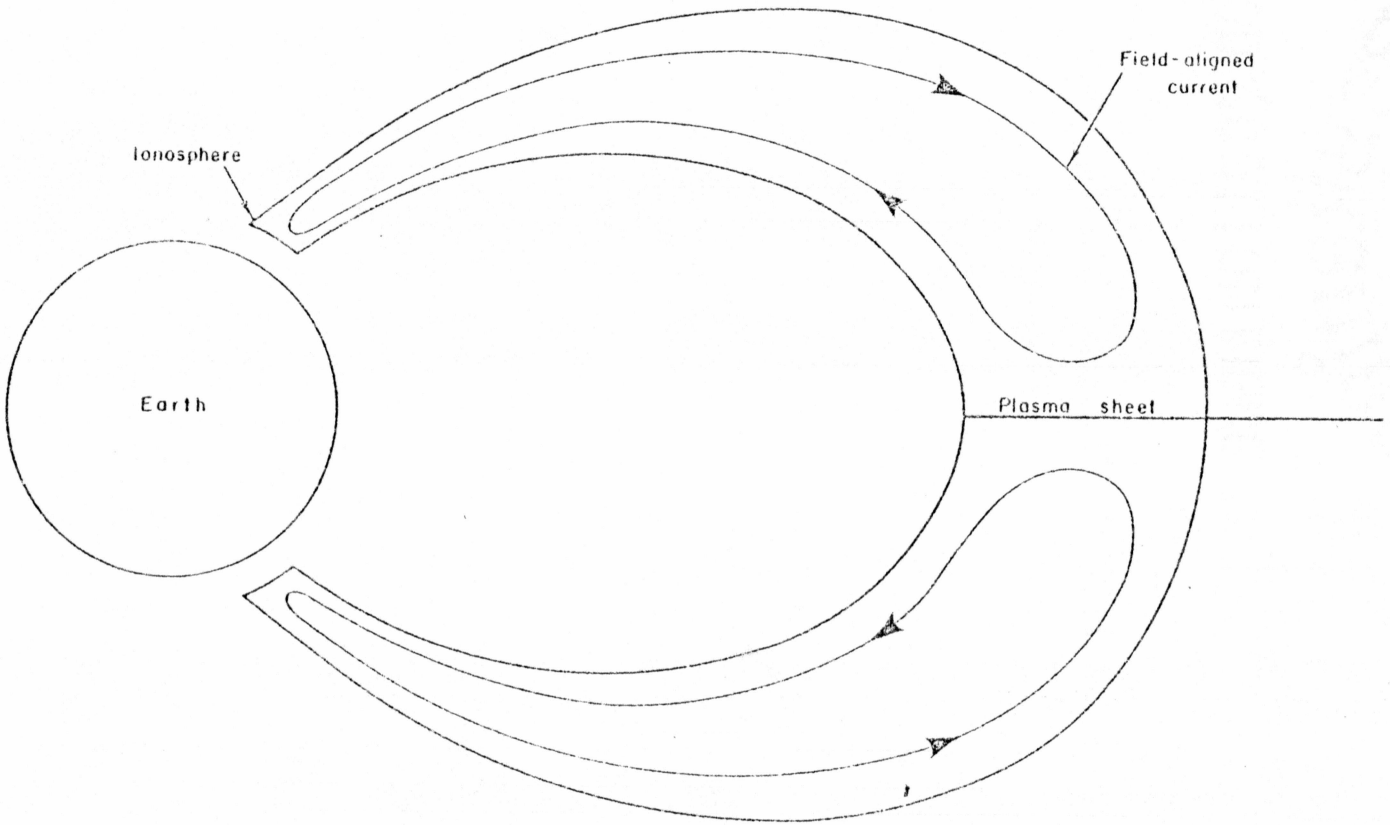

Fig. (2.1) Schematic representation of the magnetospheric-ionospheric coupling.

decreased plasma flow is known as the deceleration of magnetospheric convection.

This chapter is essentially a review of a paper by Kan et al., (1982a). It will describe the process by which they show the deceleration of magnetospheric convection can destablize MHD waves. In particular, Alfven waves can be generated which have an increasing growth rate as the convection speed increases or as the Pedersen conductivity increases. This has been proposed as a possible source of Pi pulsations (Campbell, 1967; Saito, 1969; McPherron and Coleman, 1970; Jacobs, 1970; Gendrin, 1970; Southwood and Stuart, 1980; Sakurai, 1981; Yumoto et al., 1981; Heacock and Hunsucker, 1981).

2.2 One-Dimensional Model of the Magnetospheric Dynamo Region

The region in the magnetosphere-ionosphere coupling system where the deceleration takes place will be called the magnetospheric dynamo region. In the magnetospheric dynamo $\vec{J} \cdot \vec{E}_o < 0$, where $\vec{J}$ is the dynamo current and $\vec{E}_o$ is the convection electric field (Rostoker and Bostrom, 1976).

The dynamo region will be considered quasistatic, one-dimensional and with y-dependence only. The x-axis is positive in the north direction, z is positive upwards in the northern hemisphere. The $y = 0$ plane is in the midnight meridian and the $z = 0$ plane is at the equator. See Fig. (2.2). We assume that there is no magnetic field

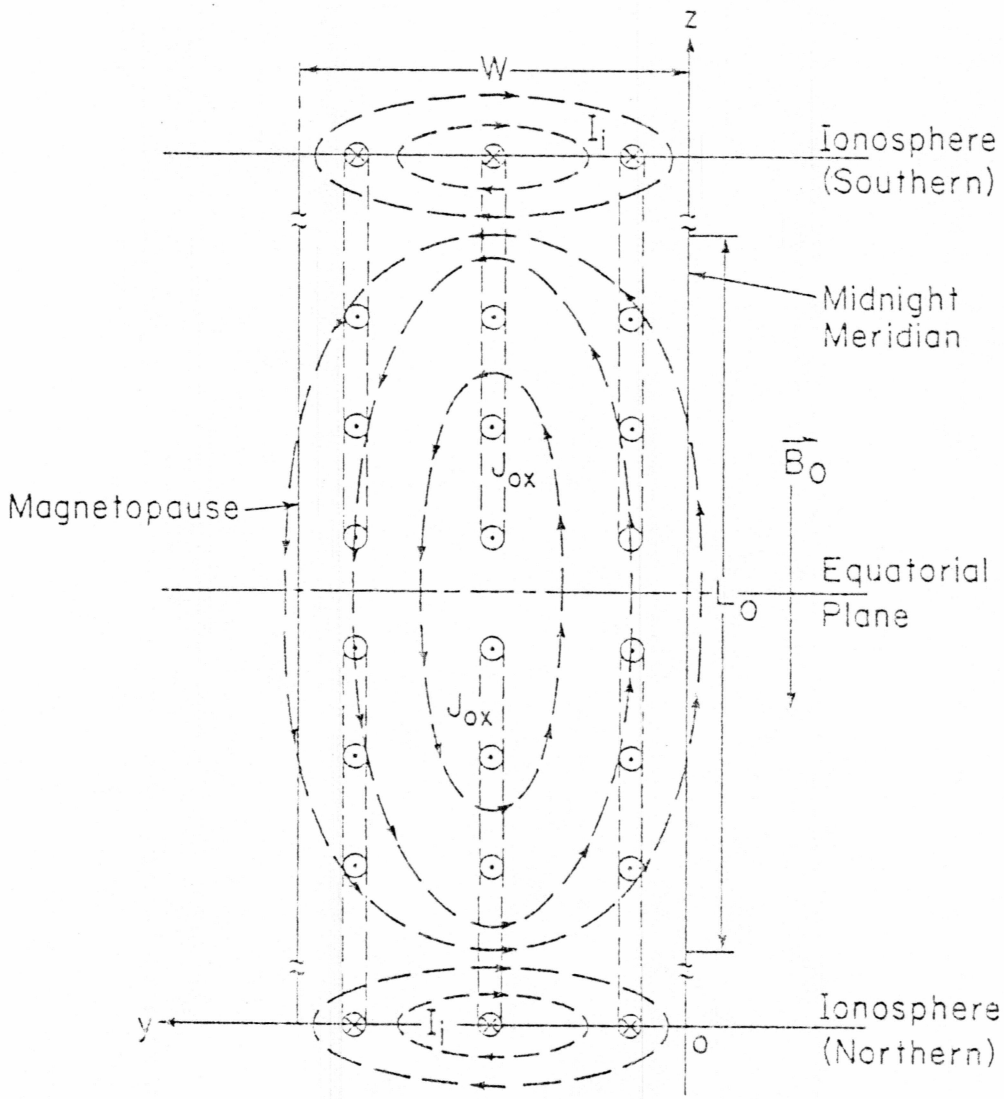

Fig. (2.2) Current loops form two solenoids of lenght W, one in each hemisphere. The dashed lines represent the magnetic field formed by the solenoids.

line convergence.

The electric field is in the north-south direction: $\vec{E} = E_o \vec{x}$. Faraday's law implies that E_{ox} = constant.

In reality the convection electric field is not one-dimensional. The observed north-south component of the convection electric field changes sign across the midnight region (e.g. Heelis and Hanson, 1980). In the evening sector the upward field-aligned currents are poleward of the downward field-aligned currents. This pattern is reversed in the morning sector. Observed polarity reversals in the field-aligned currents across the midnight region indicate that currents are partially closed by north-south Pedersen currents. The current loops are in the north-south plane. There are two solenoids, one in the northern hemisphere, the other in the southern hemisphere. The magnetic field is predominantly in the z-direction in the dynamo region. The dynamo region is delineated by W and L in Fig. (2.2). The width of the dynamo region is W and its length is L. Because of the finite width of the solenoids, the B_z component is dominant in the dynamo region. The dynamo current J_{ox} is distributed over L. The ionospheric current which closes the loop is a sheet current.

To model the current system of Fig. (2.2) we assume that the height-integrated Pedersen current is constant within the dynamo region and zero outside, i.e.,

$$\begin{aligned} \Sigma_P &= \text{constant} \qquad 0 \leq y \leq W \\ &= 0 \qquad\qquad\quad \text{otherwise.} \end{aligned} \tag{2.1}$$

Since the model is independant of z, the model can be used for the dynamo region if $L > W$.

Continuity of current in the north-south loops can be expressed by:

$$J_{ox} = - \Sigma_p E_{ox} / (L_o / 2) \qquad (2.2)$$

where L_o is the length of the field-aligned region. J_{ox} is anti-parallel to the Pedersen current as indicated by the negative sign. J_{ox} vanishes outside of the dynamo region.

The z-component of the magnetic field can be obtained from Ampere's law:

$$\frac{dB_{oz}}{dy} = \mu_o J_{ox}. \qquad (2.3)$$

By substituting (2.2) into (2.3) and integrating one obtains the z-component of the magnetic field:

$$B_{oz} = \mu_o (2 \Sigma_p E_{ox} / L_o) (y - W/2) - B_o. \qquad (2.4)$$

Equation (2.4) gives B_{oz} for the midnight sector.

The convection velocity can be calculated using the frozen-in condition

$$\vec{v}_o = - E_{ox} / B_{oz} \vec{y} = v_{oy} \vec{y}. \qquad (2.5)$$

Equations (2.4) and (2.5) are combined to give the slowing down rate

$$\frac{dv_{oy}}{dy} = - \mu_o (2 \Sigma_p v_{oy} / L_o). \qquad (2.6)$$

For moderately disturbed conditions Σ_p = 10 mhos, v_{0y} = 200 km/sec, (2.6) gives $dv_{oy}/dy = - 8 \times 10^{-3}$/sec, with L = 20 Re.

The mass conservation equation leads to

$$\rho_o v_o = \text{constant}. \qquad (2.7)$$

For the dynamo region the time-independent momentum equation for a plasma is

$$\rho_o v_o \frac{dv_{oy}}{dy} + \frac{1}{\mu_o} B_{oz} \frac{dB_{oz}}{dy} + \nabla P_o = 0. \qquad (2.8)$$

Since $\rho_o v_o$ = const, equation (2.8) can be integrated to yield

$$\rho_o v_{oy}^2 + \frac{B_{oz}^2}{2 \mu_o} + P_o = \text{constant}. \qquad (2.9)$$

The equilibrium of the system can be viewed as a configuration in which fluid plasma is supported by gravity. The deceleration rate is equivalent to the gravitational force in the - y direction. From (2.7) the density gradient can be written as

$$\frac{d\rho_o}{dy} = - \frac{F_o}{v_{oy}^2} \frac{dv_{oy}}{dy}.$$

Since dv_{oy}/dy is less than zero, $d\rho_o/dy$ is in the positive direction. Hence the "gravitational force" is opposite the density gradient which is the condition for Rayleigh-Taylor instability (Krall and Trivelpiece, 1973). There is no threshold on the size of the density gradient or the gravitational force in the absence of boundary effects. Therefore we can expect the one-dimensional dynamo region to be unstable to hydromagnetic waves.

2.3 Local Instability Analysis of the Dynamo Region

We now consider the stability of the one-dimensional dynamo region to MHD waves under the local approximation. This method of solution assumes that plasma variables such as $\vec{B}$ and $\vec{E}$ etc. can be replaced by a linear series expansion of that variable, i.e.

$$\vec{B} = \vec{B}_0 + \vec{B}_1 e^{i(\vec{k}\cdot\vec{x} - \omega t)}$$

Futhermore, the solution method is refered to as local because the coefficients $\vec{B}_0$ and $\vec{B}_1$ are independent of $\vec{x}$. The non-MHD effect of $E_{\parallel} \neq 0$ will be neglected.

Under the local approximation perturbations will be a two-dimensional wave, i.e.,

$$\xi \sim \exp(ik_x x + ik_z z - i\omega t). \tag{2.10}$$

The governing equations of linear MHD stability analysis are given by Krall and Trivelpiece (1973, p. 243):

$$\frac{\partial \rho'}{\partial t} = -\rho_o \nabla \cdot \vec{v}' - v_y' \frac{\partial \rho_o}{\partial y} - \rho' \frac{\partial v_{oy}}{\partial y} \tag{2.11}$$

$$\rho_o \frac{\partial \vec{v}'}{\partial t} + \rho_o (\vec{v}_o \cdot \nabla) v' + \rho_o (\vec{v}' \cdot \nabla) \vec{v}_o + \rho' (\vec{v}_o \cdot \nabla) \vec{v}_o$$

$$= \vec{J}_o \times \vec{B}' + \vec{J}' \times \vec{B}_o - \nabla p' \tag{2.12}$$

$$\nabla \times \vec{B}' = \mu_o \vec{J}' \tag{2.13}$$

$$\nabla \times \vec{E}_\perp = -\frac{\partial \vec{B}'}{\partial t} \tag{2.14}$$

$$\vec{E}_\perp' + \vec{v}' \times \vec{B}_o + \vec{v}_o \times \vec{B}' = 0 \tag{2.15}$$

$$p' = -\gamma p_o \rho'/\rho_o = c_s^2 \rho' \tag{2.16}$$

where γ is the ratio of specific heats and c_s is the sound speed. Substituting for $\vec{E}_\perp$ in (2.14) from (2.15) gives the expressions for $\vec{B}'$.

$$B_x' = -(k_z/\omega) B_{oz} v_x'$$

$$B_y' = -(k_z/\omega)\, B_{oz}\, v_y' \tag{2.17}$$

$$B_z' = (k_z/\omega)\, B_{oz}\, v_x'$$

Substituting this result for $\vec{B}'$ into (2.13) yields the expression for $\vec{J}'$.

$$J_x' = (ik_z^2/\mu_o\,\omega)\, B_{oz}\, v_y'$$

$$J_z' = [-i(k_x^2 + k_z^2)/\mu_o\,\omega]\, B_{oz}\, v_x' \tag{2.18}$$

$$J_z' = [-ik_xk_z/\mu_o\,\omega]\, B_{oz}\, v_y'$$

From (2.11) ρ' can be written as

$$\rho' = \frac{\rho_o}{\omega^*}\,(ik_x v_x' + ik_z v_z' + \frac{\dot{\rho}_o}{\rho_o} v_y') \tag{2.19}$$

where $\omega^* = i\omega - \dot{v}_{oy}$, $\dot{v}_{oy} = dv_{oy}/dy$ and $\dot{\rho}_o = d\rho_o/dy$. By substituting equation (2.16) through (2.19) into equation (2.12), three coupled equations for v_x', v_y' and v_z' are obtained,

$$a_{xi}\, v_x' + a_{yi}\, v_y' + a_{zi}\, v_z' = 0, \tag{2.20}$$

where, for i = 1,2,3

zero the modes are modified and the frequency becomes complex.

Since we are interested in generating Alfven waves we will look at the modes in the cold plasma ($c_s = 0$) limit. In the cold plasma limit the Alfven and fast modes are decoupled.

The characteristics of the Alfven mode can be seen when $c_s = 0$. The dispersion relation becomes

$$\omega^4 + 2_i \dot{V}_{oy} \omega^3 - (2 \dot{V}_{oy}^2 + k_z^2 V_A^2) \omega^2$$

$$- ik_z^2 V_A^2 \dot{V}_{oy} \omega - k_z^2 V_A^2 \dot{V}_{oy} = 0. \qquad (2.21)$$

For moderately oblique propagation ($\theta < 90^\circ$) $k_z \cdot V_A \gg |\dot{V}_{oy}|$ can be satisfied by Alfven waves in the Pi pulsation range. This can be ascertained by noting that $k_z \cdot V_A = \omega_r = 2\pi \times 10^{-2}$/sec and $\dot{V}_{oy} = -8 \times 10^{-3}$/sec. Therefore, ω can be approximated by

$$\omega \approx k_z V_A + \tilde{\omega}$$

and treat $\tilde{\omega}$ and $\dot{V}_{oy}$ as first order quantities in equation (2.21). Keeping first order terms one gets from (2.21)

$$\tilde{\omega} = -1 \dot{V}_{oy}/2. \qquad (2.22)$$

Hence, for moderately oblique propagation

$$\omega = \omega_r + i\omega = k_z V_A - i \dot{V}_{oy}/2. \qquad (2.23)$$

For highly perpendicular propagation $k_z/k_x \to 0$ and (2.21) yields

$$\omega = \pm \dot{V}_{oy} - i \dot{V}_{oy}. \qquad (2.24)$$

Equations (2.23) and (2.24) show that Alfven waves are unstable for $\dot{V}_{oy} < 0$. The growth rate increases by a factor or two as $k_z \to 0$. Fig. (2.3) shows the numerical solution of (2.21) for complex frequency as a function of k_z. Alfven waves can propagate perpendicular to the magnetic field.

The group velocity of the Alfven wave can be shown to be parallel to the magnetic field. Equation (2.21) is independent of k_x. The frequency is therefore independent of k_x. The group velocity defined by $v_g = d\omega_r/dk$ is parallel to the z-axis and therefore the group velocity is parallel to the magnetic field since the field is in the z-direction.

Fig. (2.4) is a polar plot showing the dependence of $\omega_r/k\ V_A$ and $\omega_i/k\ V_A$ on the propagation angle, the angle between $\vec{k}$ and $\vec{B}_o$ for $\dot{V}_{oy} = -0.05\ k\ V_A$.

For MHD waves in which $c_s \neq 0$, the general dispersion relation from the determinant of (2.20) must be solved. The values $\dot{V}_{oy} = -0.05\ kV_A$, $V_{oy} = 0.2\ V_A$ and $c_s = 0.4\ V_A$ are used. Fig. (2.5) consists of polar

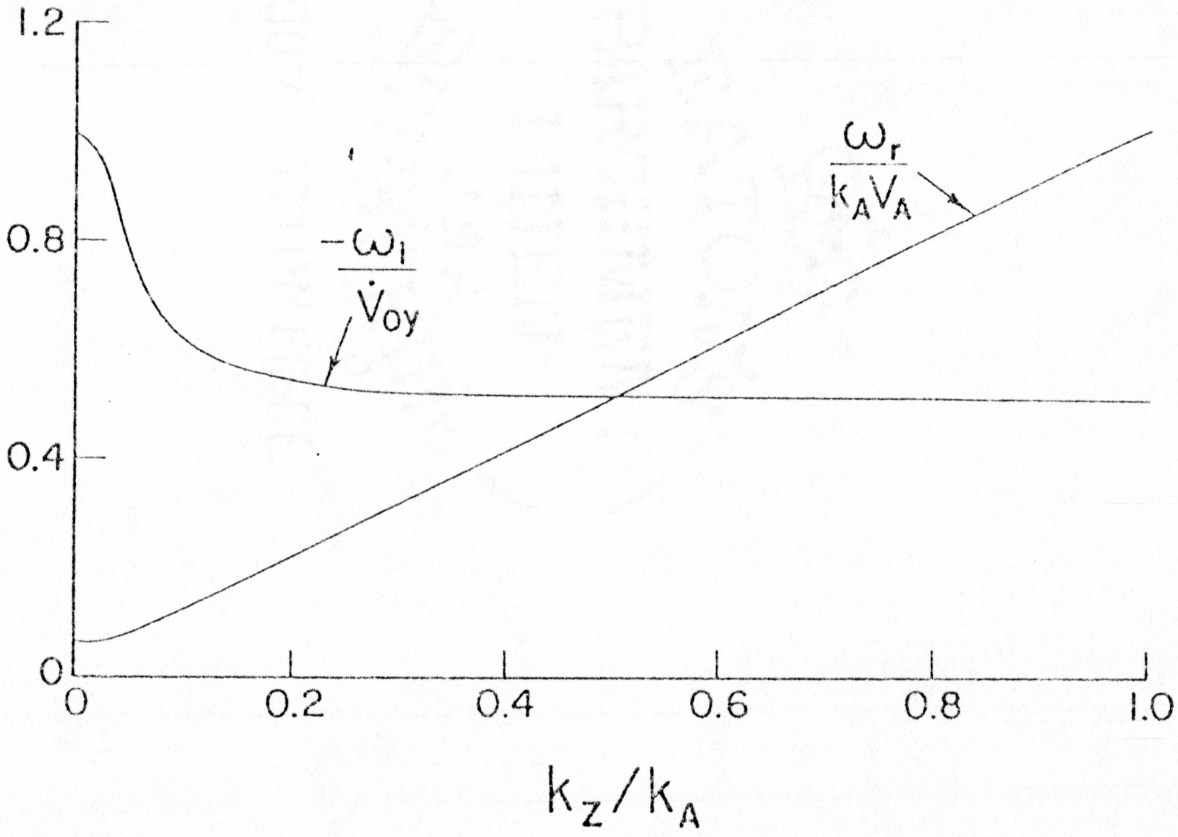

Fig. (2.3) Dispersion relation for the modified Alfven waves (complex frequency versus the wave number k_z) for $\dot{V}_{oy} = -4.0 \times 10^{-3}/s$, $k_A V_A = 2\pi \times 10^{-2}/s$, $c_s = 0$.

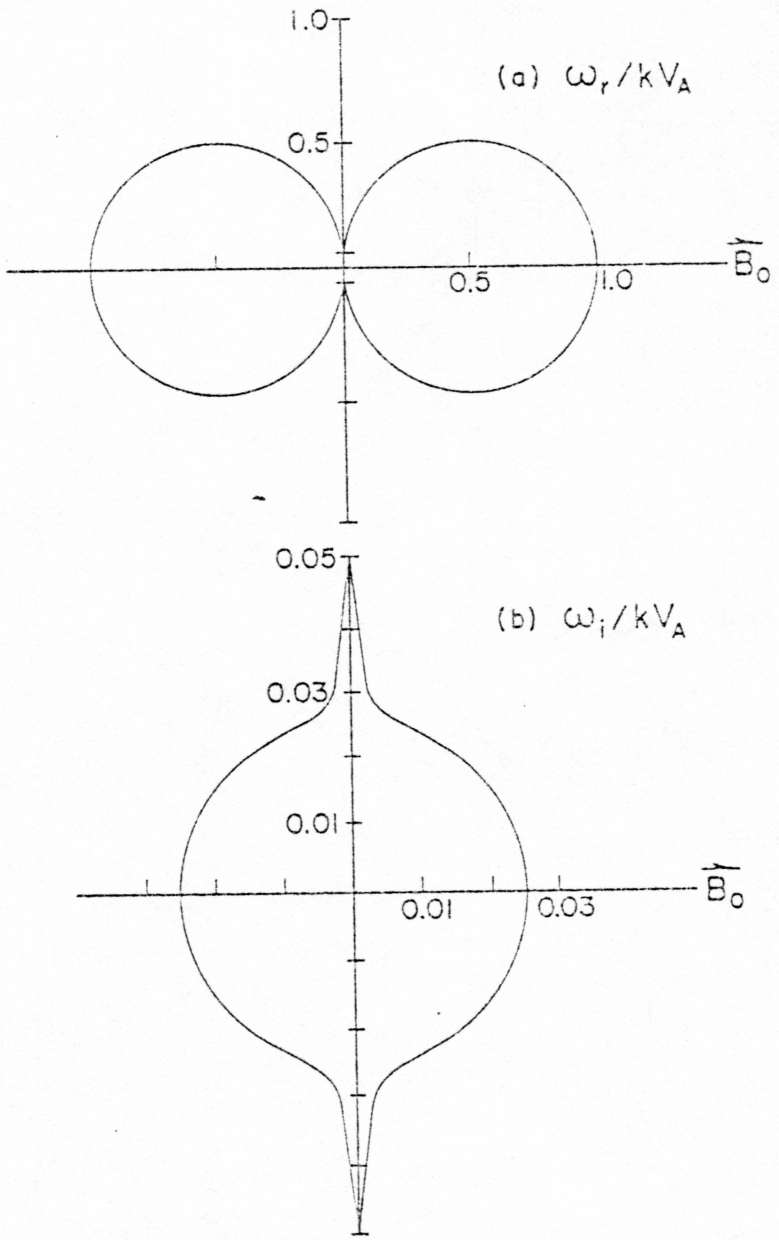

Fig. (2.4) Polar plot showing the dependence of $\omega_r kV_A$ and ω_i/kV_A on the propagation angle.

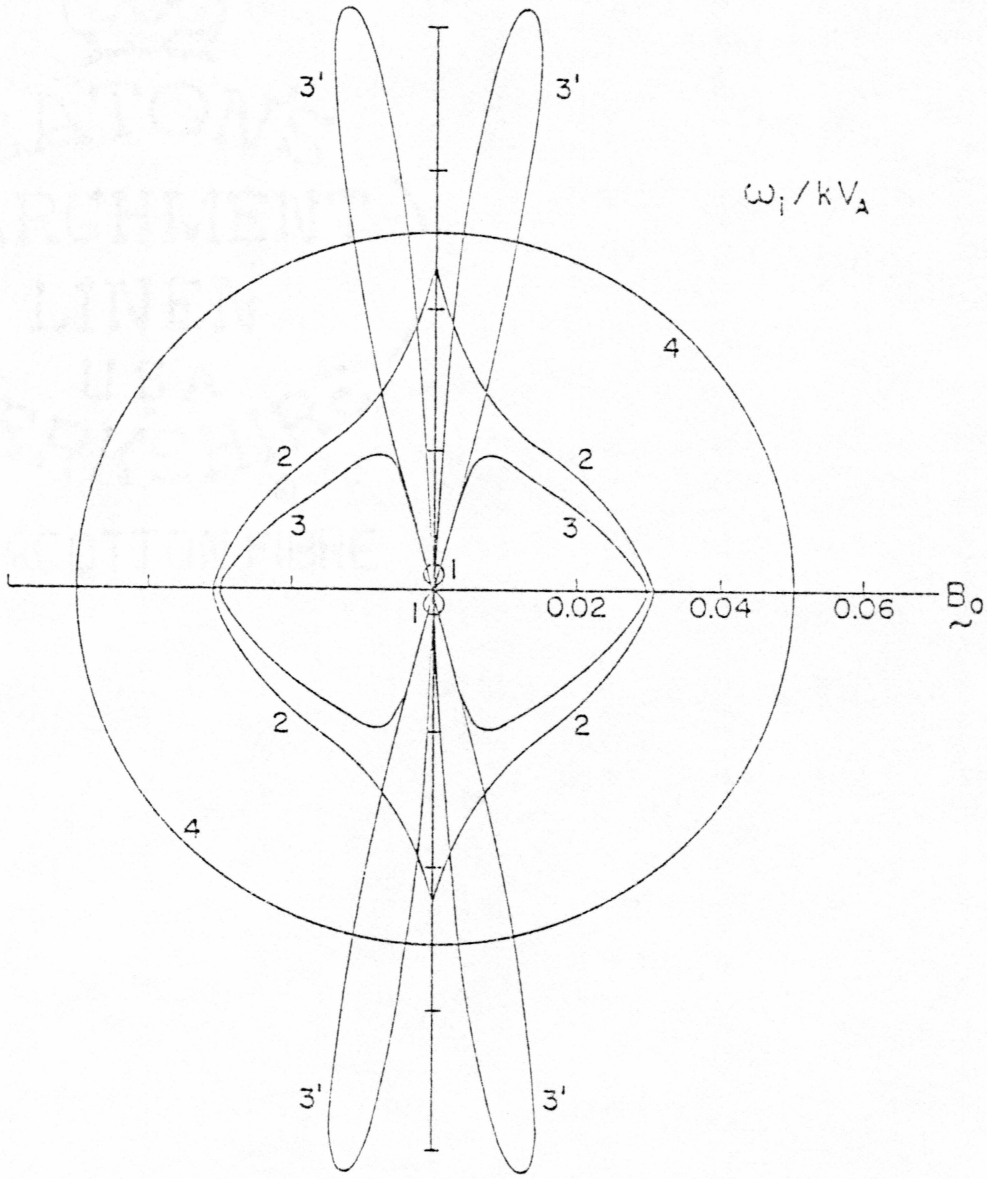

Fig. (2.5a) Polar plot of the phase velocity in constant k. The parameter values are $c_s = 0.4\ V_A$, $V_{oy} = 0.2V_A$, and $V_{oy} = -0.05kV_A$.

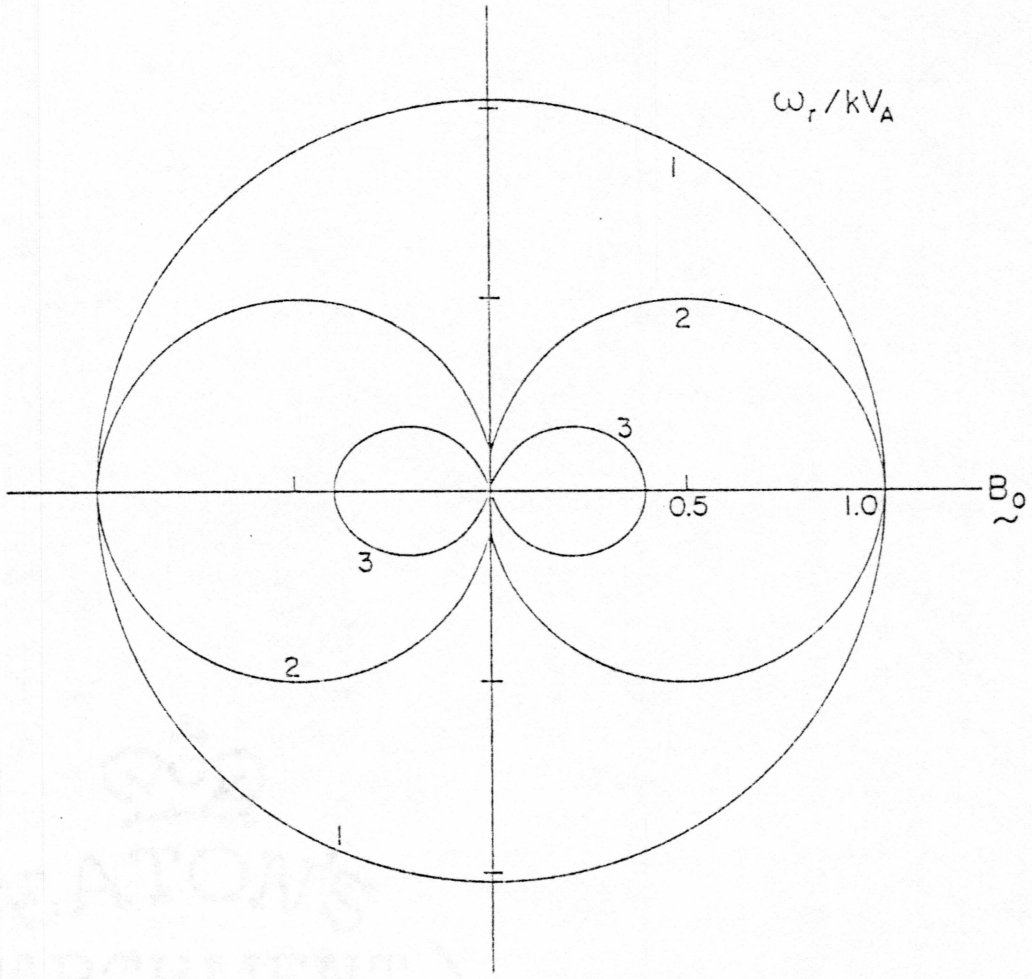

Fig. (2.5b) Polar plot showing growth rate in constant k. The parameters are the same as in Fig. (2.5a).

plots similar to Fig. (2.5). Curve 1 is the fast mode, curve 2 is the Alfven mode, curve 3 is the slow mode and curve 4 is a nonpropagating, pure growing entropy wave (Kalikhman, 1967). Figs. (2.5a) and (2.5b) contain information on wave frequency and growth rates for constant deceleration for a constant wave number k. For the fast mode k is almost constant for a given ω. It has a negative growth rate which implies that it is stable for a constant deceleration rate. The Alfven mode differs only slightly from the $c_s = 0$ case. The propagation is almost the same. From this we can conlude that Alfven waves are guided along field lines. The slow mode is unstable. The deceleration rate is proportional to k and for constant ω, decreases with increasing θ. Hence, we have the growth rate for oblique propagation. The growth rate for oblique slow mode waves is reduced from the values in Fig. (2.5b).

2.4 Overall Growth Rate of an Alfven Wave Packet Bouncing Between Hemispheres

We will now consider the overall growth rate of an Alfven wave packet which is bouncing between hemispheres. When the Alfven packet encounters the ionosphere, some of the energy is absorbed and some of the energy is reflected by the ionosphere. This effect is due to the finite ionospheric conductivity. The reflected wave is amplified by the magnetosphere and damped upon reflection. The overall averaged growth rate can be estimated.

The upgoing and downgoing waves are related by the reflection coefficient R (e.g. Maltsev et al., 1974; Mallinckrodt and Carlson, 1978; Goertz and Boswell, 1979),

$$E_u = R\, E_d .$$

The associated field-aligned currents are

$$I_d = \Sigma_m E_d$$

$$I_u = -\Sigma_n E_u$$

where $\Sigma_m = (\mu_o V_A)^{-1}$ is the mapped flux tube conductivity (Mallinckrodt and Carlson, 1978). Assuming the field-aligned currents are closed by the Pedersen current only, we have

$$I_d + I_u = I_p = \Sigma_p (E_d + e_u).$$

By combining the last four equtions the expression for R is obtained:

$$R = \frac{\Sigma_m - \Sigma_p}{\Sigma_m + \Sigma_p}. \qquad (2.25)$$

The overall growth rate is the average of the growth rate ω_i in the dynamo region and the damping rate in the ionosphere. The change in energy of the wave after being reflected by the ionosphere is

$$\Delta\varepsilon = (R\, E_d e^{\omega_i T_o})^2 - E_d^2 ,$$

where $T_o = L/V_A$, the travel time. This must equal the energy gain calculated from the net growth rate γ,

$$\Delta\varepsilon = (E_d e^{\gamma T_b})^2 - E_d^2 ,$$

where $T_b = e/V_A$, and ℓ is the field line length between the hemispheres. Equating these two expressions yields

$$E_d^2\, e^{2\gamma T_b} = R^2\, E_d^2\, e^{2\omega_i T_o} . \qquad (2.26)$$

This can be solved for γ:

$$\gamma = \omega_i\, (T_o/T_b) + (\ln R^2)/2\, T_b . \qquad (2.27)$$

The second term on the right is the ionosphere damping rate.

We now examine the growth rate for Alfven waves in the limit of $c_s = 0$. The average value of the magnetospheric conductivity for invariant latitude of 70° is $\Sigma_m = 0.5$ mho. The Pedersen conductivity for moderately disturbed conditions is $\Sigma_p = 10$ mho. For these values of the conductivities the ratio $\Sigma_m/\Sigma_p \ll 1$. The second term on the right-hand side of (2.27) can be approximated by

$$(\ln R^2)/2\ T_b = -2\Sigma_m\ V_A/\Sigma_p\ \ell = -2/(\mu_o \Sigma_p \ell). \qquad (2.28)$$

This result is in agreement with the ionospheric damping rate as given by Newton et al. (1978).

From equations (2.22) through (2.24) and Fig. (2.3) in the $c_s = 0$ limit the growth rate in the dynamo region is

$$\omega_i = -\alpha(k_z)\ \dot{V}_{oy} = 2\alpha(V_z)\ \mu_o\ \Sigma_p\ V_{oy}^2/L_o. \qquad (2.29)$$

By substituting (2.28) and (2.29) into (2.27) the average growth rate can be found

$$\gamma = \frac{2}{\mu_o\ \Sigma_p \ell}\ [\alpha\ (k_z)\ \mu_o^2\ \Sigma_p^2\ V_{oy}^2 - 1]. \qquad (2.30)$$

The necessary and sufficient condition for unstable waves bouncing between hemispheres is given by

$$\Sigma_p\ V_{oy} > \frac{1}{\mu_o \sqrt{\alpha}} = 10^6 \text{ (in MKS units)}.$$

For $\Sigma_p = 10$ mho unstable Alfven waves occur when V_{oy} exceeds 150 km/sec. Convection speeds of this magnitude have been reported by Hones et al. (1976).

The mechanism presented in this chapter generates Alfven waves in the magnetosphere by deceleration of magnetospheric plasma along field lines. The growth rate of the Alfven wave packets is proportional to

Σ_p and v_{oy}. Both of these are observed to be enhanced along field lines.

The growth rate is independent of frequency in the Pi range. As seen from Fig. (2.3), ω_i = const for $k_z \geq 0.2\ k_A$. The corresponding real component of the frequency ω_r is $k_z V_A \geq .2\ k_A V_A = \frac{2\pi}{500}$/sec. Since $k_A V_A = \frac{2\pi}{100}$/sec in Fig. (2.3) the growth rate is independent of the wave frequency for T $\leq$ 500 sec when contains the Pi 2 range. This means that this mechanism can generate a broad range of frequencies.

III TRANSIENT RESPONSE OF THE MAGNETOSPHERE-IONOSPHERE COUPLING TO AN ENHANCEMENT OF MAGNETOSPHERIC CONVECTION

3.1 Introduction

In this chapter a derivation of the one-dimensional wave equation which describes magnetosphere-ionosphere coupling based on the MHD equations is given. This equation can be used to determine the field-aligned currents and the electric field in the auroral ionosphere for a given potential difference across field lines applied at the plasma sheet in the magnetosphere. This equation will be solved numerically and the results will be discussed.

3.2 Derivation of Wave Equation

The wave equation is solved for the magnetosphere-ionosphere coupling (Miura and Sato, 1980; Sato, 1978; Sato and Holtzer, 1973; Holtzer and Sato, 1973; Ogawa and Sato, 1971; Atkinson, 1970). It is assumed that the magnetic field and the density are constant along the magnetic field lines and equal to their average values. Field line curvature is neglected. The test of the validity of the use of the MHD equations under these assumptions is given in the appendix.

and Sato (1980). The MHD equations for a cold, incompressible infinite conducting plasma (Krall and Trivelpiece, 1973) are:

$$\nabla \cdot \vec{v} = 0 \tag{3.1}$$

$$\rho \frac{\partial \vec{v}}{\partial t} = \vec{J} \times \vec{B} \tag{3.2}$$

$$\vec{E} + \vec{v} \times \vec{B} = 0 \tag{3.3}$$

$$\nabla \times \vec{E} = - \frac{\partial \vec{B}}{\partial \vec{t}} \tag{3.4}$$

$$\nabla \times \vec{B} = \mu_o \vec{J}. \tag{3.5}$$

They are respectively the equation of continuity, the momentum transport equation, Ohm's law, Faraday's law, and Ampere's law.

This set of equations is solved by the method of linearization. This is accomplished by expressing each dependent variable as the sum of two terms, the equilibrium term and the perturbed term, i.e.:

$$\rho = \rho_o + \rho_1 e^{i(\vec{k} \cdot \vec{x} - \omega t)}.$$

These are substituted into the equations above. All quantities which involve the product of two perturbed variables are neglected. We assume that the initial velocity is zero, the initial current is zero, and the magnetic field is in the z-direction. With these assumptions eqs. (3.2)

to (3.5) become

$$\rho_o \frac{\partial \vec{v}_1}{\partial t} = \vec{J}_1 \times \vec{B}_o \tag{3.6}$$

$$\vec{E}_1 + \vec{v}_1 \times \vec{B}_o = 0 \tag{3.7}$$

$$\nabla \times \vec{E}_1 = - \frac{\partial \vec{B}_1}{\partial t} \tag{3.8}$$

$$\nabla \times \vec{B}_1 = \mu_o \vec{J}_1 . \tag{3.9}$$

After taking the curl of (3.8) and substituting for the curl of B from (3.9), we get an equation with the use of the vector identity $\nabla \times \nabla \times \vec{F} = \nabla (\nabla \cdot \vec{F}) - \nabla^2 \vec{F}$ relating E and J:

$$\nabla (\nabla \cdot \vec{E}_1) - \nabla^2 \vec{E}_1 = - \frac{\partial}{\partial t} (\mu_o \vec{J}) . \tag{3.10}$$

Due to the infinite conductivity along the field lines, there is no parallel component of the electric field. By taking the parallel component of (3.10) we get an equation relating the electric field to the parallel current

$$\frac{\partial}{\partial z} (\nabla \cdot \vec{E}) = - \frac{\partial}{\partial t} \mu_o J_{1z} . \tag{3.11}$$

The polarization current across the field comes from the momentum equation and Ohms's law. We have from equations (3.9) and (3.8):

$$\vec{v}_1 \times \vec{B}_o = - \vec{E}_1$$

$$v_{1y} = \frac{E_{1x}}{B_o}$$

$$v_{1x} = \frac{E_{1y}}{B_o}.$$

Upon substituting this into (3.6) we get for the x and y components respectively

$$\rho_o \frac{\partial}{\partial t} (E_{1y}/B_o) = J_{1y} B_o$$

$$\rho_o \frac{\partial}{\partial t} (- E_{1x}/B_o) = - J_{1x} B_o.$$

Combining these two equations yields

$$\rho_o \frac{\partial \vec{E}_1}{\partial t} = \vec{J}_{1\perp} B_o^2. \qquad (3.12)$$

Under the assumption that the density does not depend on the perpendicular distance from the field line the divergence of (3.12) becomes

$$\frac{\rho_o}{B_o^2} \frac{\partial}{\partial t} (\nabla \cdot \vec{E}_1) = \nabla \cdot \vec{J}_{1\perp}. \qquad (3.13)$$

The three-dimensional current continuity equation is used to express the

perpendicular component in terms of the parallel component:

$$\nabla \cdot \vec{J}_1 = \nabla_\perp \cdot \vec{J}_{1\perp} + \frac{\partial}{\partial z} J_{1z}.$$

Upon substitution we get

$$\frac{\rho_o}{B_o^2} \frac{\partial}{\partial t} (\nabla \cdot \vec{E}_1) = - \frac{\partial}{\partial z} J_{1z}. \qquad (3.14)$$

By taking $\partial/\partial z$ of (3.11) and $\partial/\partial t$ of (3.14) and combining the results we get the one dimensional wave equation for $\nabla \cdot \vec{E}_1$ after eliminating J_{1z},

$$\frac{\partial^2}{\partial t^2} (\nabla \cdot \vec{E}_1) - v_A^2 \frac{\partial^2}{\partial z^2} (\nabla \cdot \vec{E}_1) = 0. \qquad (3.15)$$

where $v_A^2 = B_o^2 / \rho_o \mu_o$. An identical equation for J_{1z} can be obtained by interchanging the partial derivatives above and eliminating J_{1z}. In the magnetosphere the Alfven wave will be non-linear, and therefore a non-linear treatment of the MHD equations is required. However, the non-linear derivation yields the same one-dimensional equation (Kan et al., 1982b).

In this section we have derived a one-dimensional wave equation for the magnetosphere-ionosphere coupling. The basis for the derivation was the MHD equations for a cold, incompressible, infinite conducting plasma. The MHD equations were solved by the method of linearization and all second and higher order terms were neglected. The resultant equation is the one-dimensional, homogeneous wave equation.

3.3 Lax-Wendroff Algorithm

In this section the numerical method for the solution of the one-dimensional wave equation will be given. To conform to the notation used in Potter (1973), the dependent variables $\nabla \cdot \vec{E}_1$ and J_{1z} will replaced by u and F respectively and the independent variable z will replaced with x and the speed of propagation will be denoted by c.

The wave equation in the new notation is:

$$\frac{\partial^2 u}{\partial t^2} - c^2 \frac{\partial^2 u}{\partial x^2} = 0. \tag{3.16}$$

This is a one-dimensional second-order hyperbolic partial differential equation. It can be expressed as two first order partial differential equations:

$$\frac{\partial u}{\partial t} + c^2 \frac{\partial F}{\partial x} = 0 \tag{3.17}$$

$$\frac{\partial F}{\partial t} + \frac{\partial u}{\partial x} = 0. \tag{3.18}$$

The solutions for these two equations will be computed on a space-time difference grid. These equations are said to be in conservative form since they conserve the 'flux' of the system on the difference grid. The method of solution is known as the two-step Lax-Wendroff scheme.

Equation (3.16) in difference form is

$$\frac{u_j^{n+1} - u_j^n}{\Delta t} + c^2 \frac{F_{j+1}^n - F_{n+1}^n}{2\Delta} = 0,$$

where the superscripts represent the time and subscripts represent space variations, Δ is the grid spacing. This can be solved for u_j at the n+1 time step in terms of quantities at the n^{th} time step.

$$u_j^{n+1} = u_j^n - \frac{c^2 \Delta t}{2 \Delta} (F_{j+1}^n - F_{j-1}^n)$$

This explicit method is inherently unstable and therefore unsuitable for any size time step (see Potter 1973, pp. 55-56). However, if u_j^n is replaced by its spatial average the algorithm is stable and it is known as the Lax scheme:

$$u_j^{n+1} = \frac{1}{2} (u_{j+1}^n + u_{j-1}^n) - \frac{c^2 \Delta t}{2 \Delta} (F_{j+1}^n - F_{j-1}^n). \quad (3.19)$$

This method has first order accuracy in the time step. Second order accuracy can be obtained by advancing the solution in two half steps. The Lax method is used to advance the solution one-half of a step:

$$u_{j+1/2}^{n+1/2} = \frac{1}{2} (u_j^n + u_{j+1}^n) - \frac{c^2 \Delta t}{2 \Delta} (F_{j+1}^n - F_j^n).$$

This known as the auxiliary step. A similiar expression is formed for $F_{j+1/2}^{n+1/2}$. These variables are then used in the main step to determine the solution at the grid points:

$$u_j^{n+1} = u_j^n - \frac{c^2 \Delta t}{\Delta} (F_{j+1/2}^{n+1/2} - F_{j-1/2}^{n+1/2}).$$

A complete specification of the algorithm for both dependent variables is then:

auxiliary step:

$$u_{j+1/2}^{n+1/2} = \frac{1}{2} (u_j^n + u_{j+1}^n) - \frac{c^2 \Delta t}{2 \Delta} (F_{j+1}^n - F_j^n)$$

$$F_{j+1/2}^{n+1/2} = \frac{1}{2} (F_j^n + F_{j+1}^n) - \frac{\Delta t}{2 \Delta} (u_{j+1}^n - u_j^n)$$

main step:

$$u_j^{n+1} = u_j^n - \frac{c^2 \Delta t}{\Delta} (F_{j+1/2}^{n+1/2} - F_{j-1/2}^{n+1/2})$$

$$F_j^{n+1} = F_j^n - \frac{\Delta t}{\Delta} (u_{j+1/2}^{n+1/2} - u_{j-1/2}^{n+1/2}).$$

For the purpose of integration of these equations, the spatial grid is normalized. The equation which relates the position x to its normalized value is

$$x/l = s,$$

where l is the length of the system. The grid spacing, Δ, is the distance between adjacent grid points. It is determined by the total number of grid points along the spatial axis:

$$\Delta = \frac{1}{j_{max} - 1} .$$

For the method to be stable the inequality

$$\Delta t \leq \frac{\Delta}{|c|}$$

must hold, where $|c|$ is the absolute value of the fastest propagating mode (Potter, 1973, p. 69).

Before the integration of (3.17) and (3.18) can be started both dependent variables must be specified at the initial time. These are the initial conditions. However, for certain type of problems, information might only be available for one of the dependent variables. In this case (3.17) or (3.18) has to be used to determine the unknown initial condition. Consider the case when $u(x,0)$ and $u_t(x,0)$ are given. We have

$$u(x,0) = f(x)$$

$$u_t(x,0) = g(x)$$

Equation (3.17) can be written in terms of finite differences and solved for F^1_{j+1}:

$$F^1_{j+1} = F^1_j - \frac{\Delta}{c^2} g(s) .$$

The other dependent variable can be determined directly:

$$u_j^1 = f(s).$$

With the initial state of both variables specified the solution can be advanced in time by the Lax-Wendroff algorithm. Because of the time centering nature of the algorithm, the end points of the spatial axis must be handled separately. For the s = 0 boundary, which correseponds to the magnetosphere, the solution for u will be given, u(0,t) = a(t). By replacing the derivatives in (3.18) by finite differences, the solution for F at the boundary can be found

$$F_1^{n+1} = F_1^n - \frac{\Delta t}{\Delta} (u_2^n - u_1^n).$$

This method of handling the boundary will produce a solution which has the properties of a perfectly reflecting boundary. A solution which propagates along the grid will be reflected without loss of amplitude and the sign of the outgoing solution will be the negative of the incoming solution. The change of sign is produced because the solution is 'fixed' on the boundary by the boundary condition a(t).

The ionosphere partially transmits and partially reflects incoming signals. This property is due to the differences in the conductivity of the magnetosphere and the ionosphere. This difference is manifested in

the wave equations by the velocities of propagation. By adjusting the relative velocity of propagation at the interface the amount of reflection and transmission can be controlled.

To accomplish this on a finite-length grid a scheme must be devised which eventually absorbs the transmitted wave. This can be done by dividing the grid into two regions, see Fig. (3.1). A pulse is transmitted from point a. It travels to the right, hits the interface and is both reflected and transmitted. The amplitude and the phase of the secondary pulses will be determined by the values of c_1 and c_2, the propagation speeds in regions I and region II respectively. We will be concerned with what happens in region I. The plasma sheet will be at x = 0 and the ionosphere will be at x = 1. When the pulse hits the interface the transmitted wave will propagate into region II, strike the boundary and be reflected. Since we are only concerned with the physics in region I the transmitted pulse must be eliminated. This can be accopmplished by damping out the transmitted wave at the boundary.

The 'device' which is used to do this is known as a dashpot (Crawford, 1965). In a mechanical system such as a stretched string, the damping device would be a piston immersed in a viscous fluid. The wave traveling along the string would raise the piston and it would then return to its equilibrium state under the influence of gravity and the damping force of the fluid. If the viscosity of the fluid is matched perfectly with the characteristics of the string none of the pulse will be reflected at the boundary.

The equation for a dashpot can be determined with the help of Fig.

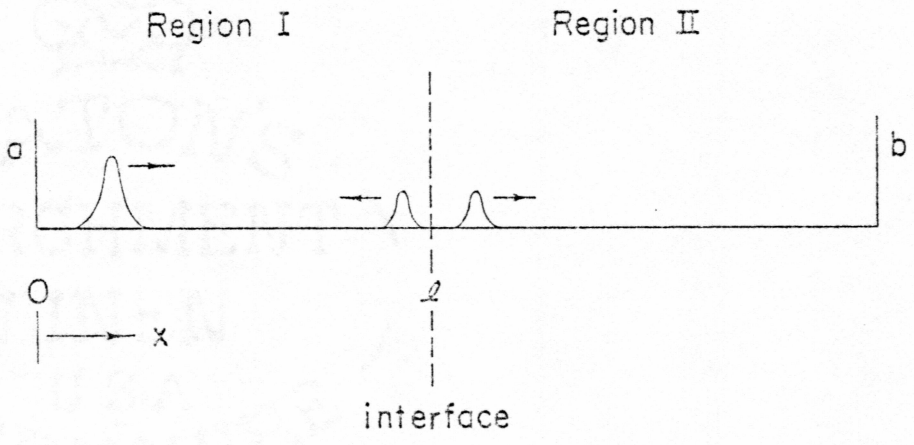

Fig. (3.1) Schematic diagram of integration region. A pulse travelling from the a will be both reflected and transmitted at the interface. Region I represents the magnetosphere-ionosphere coupling. The tramsmitted wave in Region II will be absorbed at b by a dashpot, see test.

(3.2). In the vertical direction there are two forces acting on the dashpot. The tension in the string produces the force $T\sin\theta$. If θ is small this is approximately equal $T\tan\theta$. The tangent of θ can be replaced by $-\partial u/\partial x$. The damping force is $-b\partial u/\partial t$. If the dashpot is assumed to be massless the equation for it becomes

$$T\frac{\partial u}{\partial x} + b\frac{\partial u}{\partial t} = 0.$$

Solving this for $\partial u/\partial t$ we get

$$\frac{\partial u}{\partial t} = -\frac{1}{\alpha}\frac{\partial u}{\partial x} \tag{3.20}$$

where $\alpha = b/T$. The solution of this equation will give the value of the dependent variable on the boundary.

Numerically, (3.20) is used to find u on the boundary. As in the Lax-Wendroff algorithm, the time step is divided into two steps. The auxiliary step is given by

$$u_J^{n+1/2} = -\frac{\Delta t}{2\alpha}\left(\frac{\partial u}{\partial x}\right)_J^n + u_J^n \tag{3.21}$$

where

$$\left(\frac{\partial u}{\partial x}\right)_J^n = \frac{1}{\Delta}(u_J^n - u_{J-1}^n). \tag{3.22}$$

J is the index for the last grid point. The value of u at the next-to-

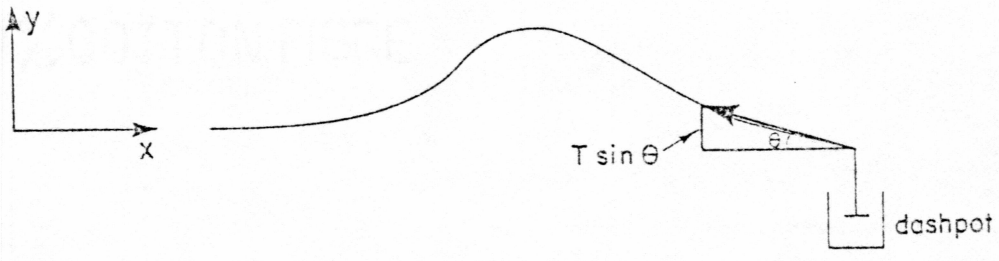

Fig. (3.2) Geometry of a pulse as it approaches the dashpot.

last grid point can be determined by the average

$$u_{J-1}^{n+1/2} = \frac{1}{2}(u_{J-1}^{n} + u_{J-1}^{n+1}). \tag{3.23}$$

Equations (3.21) and (3.23) can be used to determine the spatial derivative of u at the half-time step:

$$\left(\frac{\partial u}{\partial x}\right)_{J}^{n+1/2} = \frac{1}{\Delta}(u_{J}^{n+1/2} - u_{J-1}^{n+1/2}). \tag{3.24}$$

And now the solution on the boundary can be found from (3.20):

$$u_{J}^{n+1} = -\frac{\Delta t}{\alpha}\left(\frac{\partial u}{\partial x}\right)_{J}^{n+1/2} + u_{J}^{n}. \tag{3.25}$$

If the viscosity of the dashpot is adjusted such that $1/\alpha = v_2$, the velocity in region II, the transmitted wave will be completely absorbed at the boundary.

3.4 Computed Results

In this section computational results are given. Figs. (3.3) and (3.4) demonstrate some of the characteristics relating the enhancement of the divergence of the magnetospheric electric field, or source, to the ionospheric electric field and current, or collectively, the load. Applications to the magnetospheric-ionospheric coupling are given.

MAGNETOSPHERE

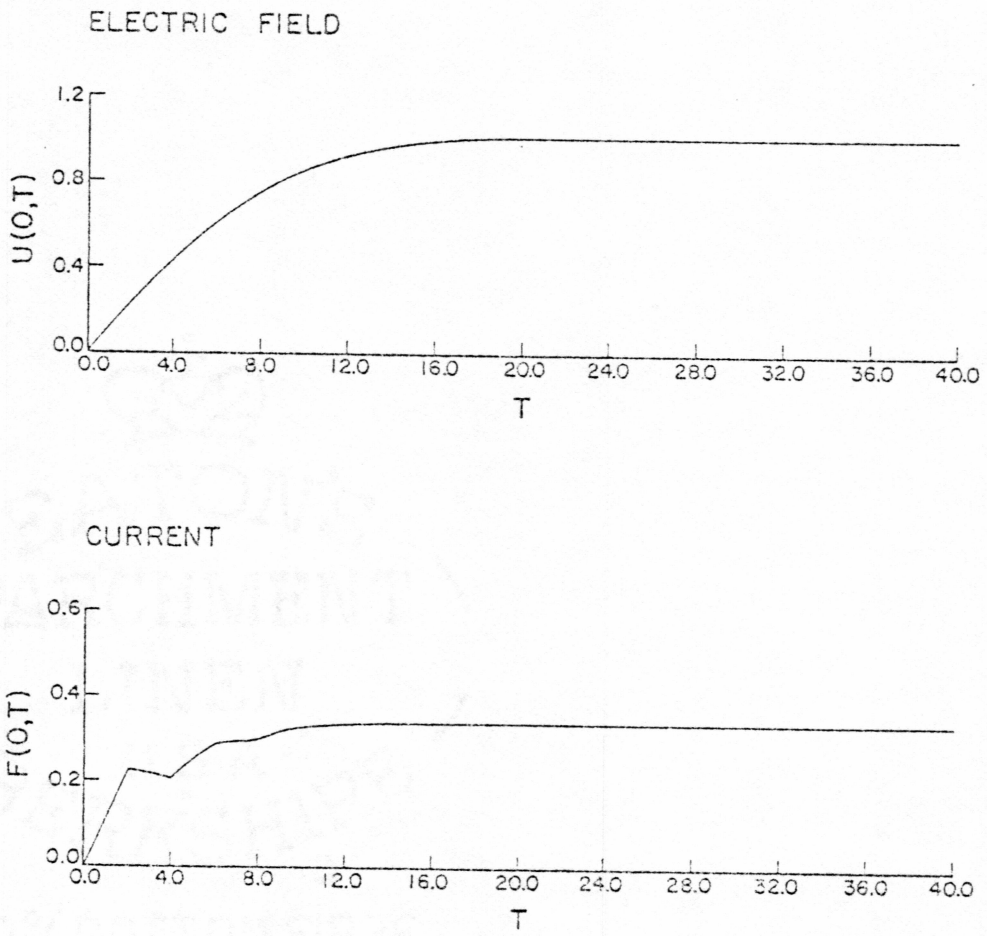

Fig. (3.3a) Plot of magnetospheric electric field and current for a gradual enhancement of the magnetospheric convection. The abscissa is in units of travel times. The ordinate is normalized to the steady state magnetospheric electric field.

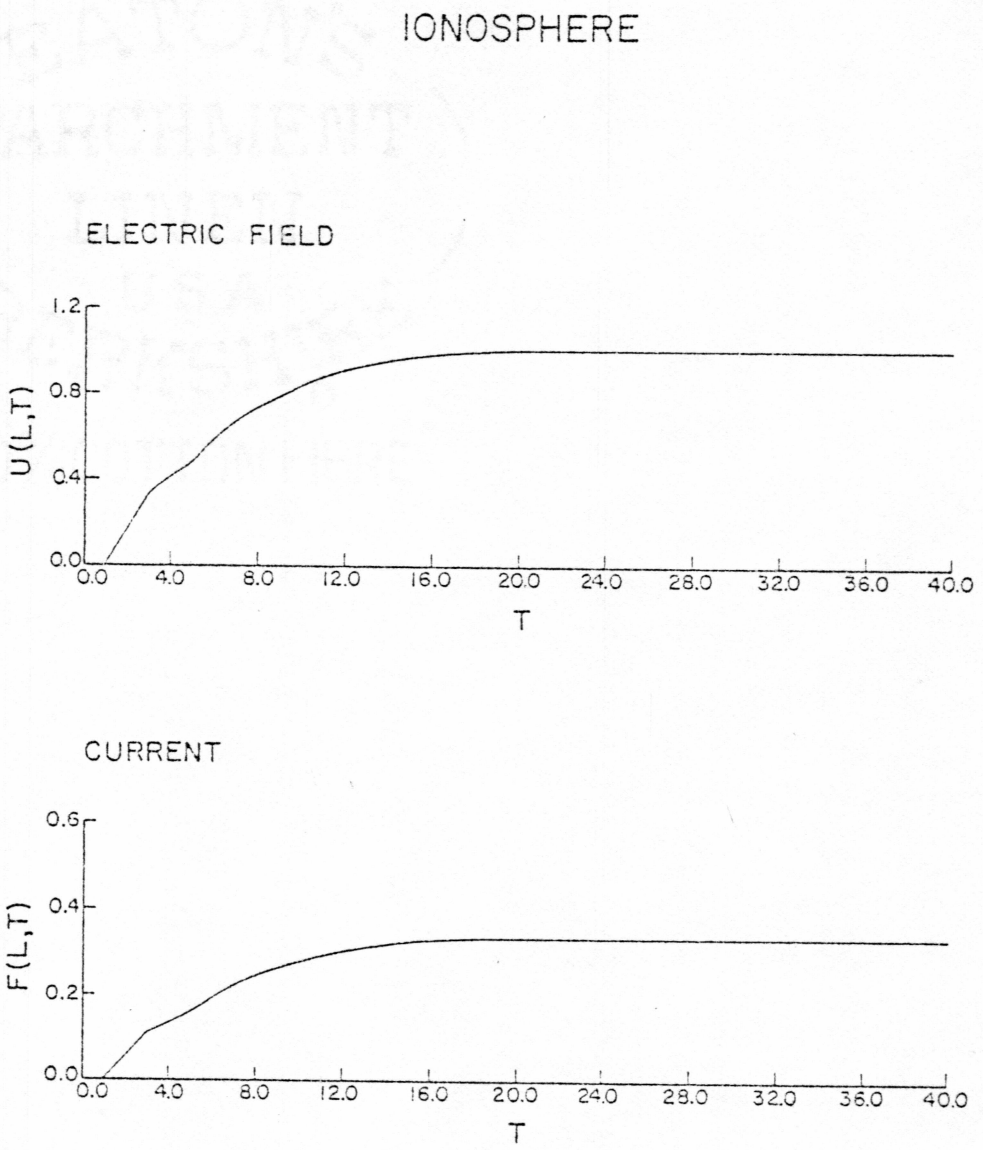

Fig. (3.3b) Plot of resultant ionospheric electric field and current for the enhancement of Fig. (3.3a).

MAGNETOSPHERE

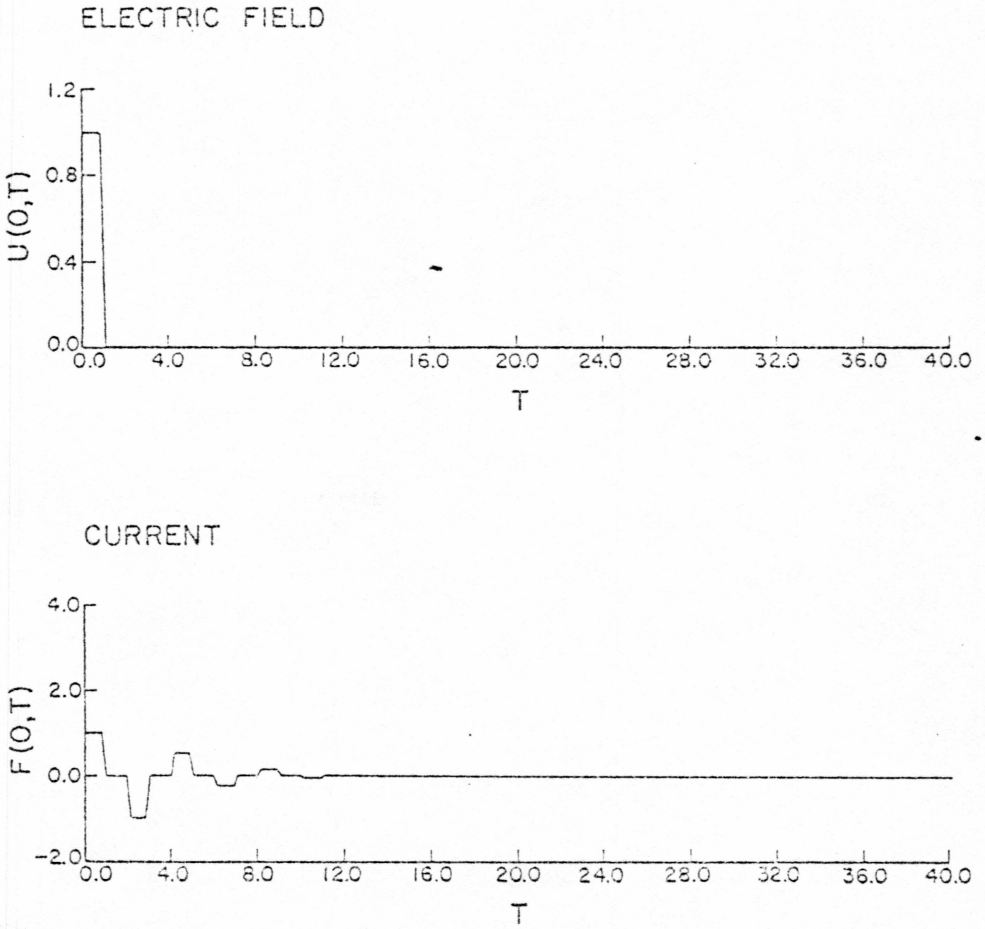

Fig. (3.4a) Plot of magnetospheric electric field and current for an instantaneous enhancement of the magnetospheric convection with a short duration. The abscissa is in units of travel times. The ordinate is normalized to the maximum magnetospheric electric field.

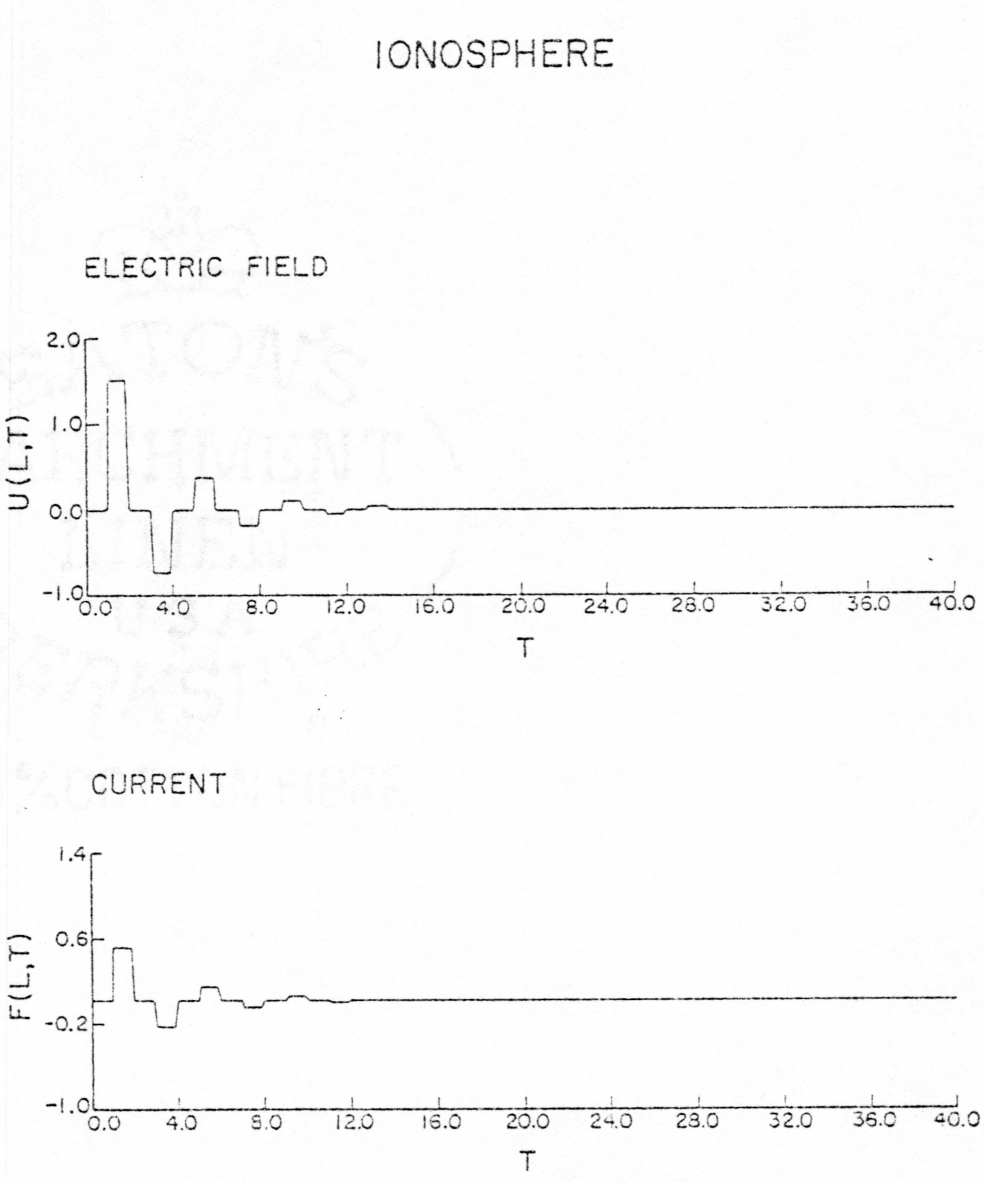

Fig. (3.4b) Plot of resultant ionospheric electric field and current for the enhancement of Fig. (3.4a).

For the remainder of this section the divergence of the electric field will be interpreted as the electric field. This is a reasonable assumption because we are only concerned with the change in the divergence of the electric field or a change in the electric field and not the absolute values of these quantities. In other words, we assume that the electric field is proportional to the divergence of the electric field.

In the magnetospheric-ionospheric coupling the power source is the plasma sheet. In the figures this will simply be labeled and refered to as the 'Magnetosphere'. The load is the auroral ionosphere and will be called the 'Ionosphere'.

The magnetosphere-ionosphere coupling is analogous to a transmission line system. Both systems are subject to reflections of currents and electric fields at both source and receiving, or load, ends. These reflections are due to a difference between the impedence of the load and the characteristic impedence of the system (cf. Johnson, 1951). For this study, we assume that the magnetospheric source is a perfect reflector (Kan et al., 1982b), and therefore the current reflection coefficient is +1 (Johnson, 1951). It has been proposed (Kan et al., 1982b) that the ionosphere must have a smaller conductivity than the magnetosphere to produce Pi 2 pulsations by enhanced magnetospheric convection. This implies that the ionospheric reflection coefficient for the electric field must be less than unity. For this study we chose the value of 1/2 for the reflection coefficient. The expression for the ionospheric reflection coefficient is given by

$$k_i = \frac{\Sigma_o - \Sigma_i}{\Sigma_o + \Sigma_i}, \qquad (3.26)$$

where Σ_o is the magnetospheric height-integrated conductivity (Akasofu and Chapman, 1972) and Σ_i is the height-integrated ionospheric conductivity. By substituting the values for k_i into equation (3.26) we get for the height-integrated ionospheric conductivity

$$\Sigma_i = \Sigma_o/3.$$

The ionospheric reflection coefficient of 1/2 will therefore satisify the requirement that the ionospheric height-integrated conductivity be less than the magnetospheric height-integrated conductivity. The reflection coefficients will remain the same for all the examples in this section.

Fig. (3.3a) shows the magnetospheric electric field and current for the case of a gradual enhancement of the magnetospheric electric field. The abscissa is in units of travel times. One travel time, T_o, is the time it takes a signal to travel from the source to the load. The ordinate is normalized to the magnetospheric steady state electric field. The enhancement is refered to as gradual because the time it takes the magnetospheric electric field to reach its steady state, the rise time, is long compared to the travel time. In this particular example the rise time is about $20T_o$. Fig. (3.3b) shows the load, or ionospheric, response to the magnetospheric enhancement. No response in

the electric field or current is seen until the time t, is greater than T_o. Both the electric field and current gradually increase and reach a steady state around the time $20T_o$.

The kinks which develop in the current plot of Fig. (3.3a) are due to current reflections which orginate at the load. The first kink is at about $t = 2T_o$, the time it takes the current to travel from the source to the load and back again. The sign of the current reflected from the load is the negative of the sign of the incoming current. For the situation in Fig. (3.3a), the reflected current is negative and upon arrival at the source it will decrease the current.

Fig. (3.4a) shows the magnetospheric electric field and current for an instantaneous enhancement of the electric field. The duration of the enhancement is about $1T_o$. Fig. (3.4b) shows the response at the ionosphere. The electric field pulse reaches the the ionosphere at $t = T_o$, and due to the reflection coefficient of 1/2, reflects an electric field pulse of $E_o/2$, where E_o is the magnitude of the magnetospheric electric field. The reflected electric field returns to the source and is rereflected. Due to the magnetosphere's reflection coefficient of -1, the rereflected electric field is $-E_o$. At $t = 3T_o$ this pulse has reached the ionosphere again. From the figure we see that the magnitude of the electric field is less than after the first reflection and that it is also negative. As T_o gets larger, the electric fields and currents are damped out and eventually the entire system is in a steady state. This example shows that a short pulse, i.e. a pulse with a rapid rise time and a short duration, propagates as a discrete packet, and is

eventually damped out.

Fig. (3.5) shows the electric fields and currents for an enhancement with a short rise time, a long duration, and a rapid decline. In Fig (3.5a) the electric field and current for the magnetosphere are plotted. The consequences of the short rise time and long duration will be examined. As in the previous figures, the ionospheric electric field and current respond to the enhancement at $t = T_o$. The ionospheric electric field rises to $1.5E_o$, where E_o is the electric field at the magnetosphere. The overshoot is again due to the ionospheric reflection coefficient of 1/2. The reflected electric field will have a value of $E_o/2$. This will be rereflected from the magnetosphere, and have a value of $-E_o/2$. Each successive pair of reflections will decrease the magnitude of the reflected wave by -1/2. The resultant electric field and current are shown in Fig. (3.5b). The effect is to produce damped oscillations of the ionospheric electric field and current which asymptotically approach the steady state.

Magnetic perturbations on the ground produced by oscillating currents in the ionosphere will also be oscillatory. The present model is one-dimensional and therefore does not have Hall currents. A two-dimensional model of the ionosphere would have both Pedersen and Hall currents. The ground observed signals would be produced by both of these currents. Fig. (3.6) shows the magnetic perturbations as recorded by the University of Alberta magnetometer chain for November 23, 1970 (Olson and Rostoker, 1975). By comparing the form of the ionospheric current in Fig. (3.5a) and the trace at MCMU, it is concluded that the

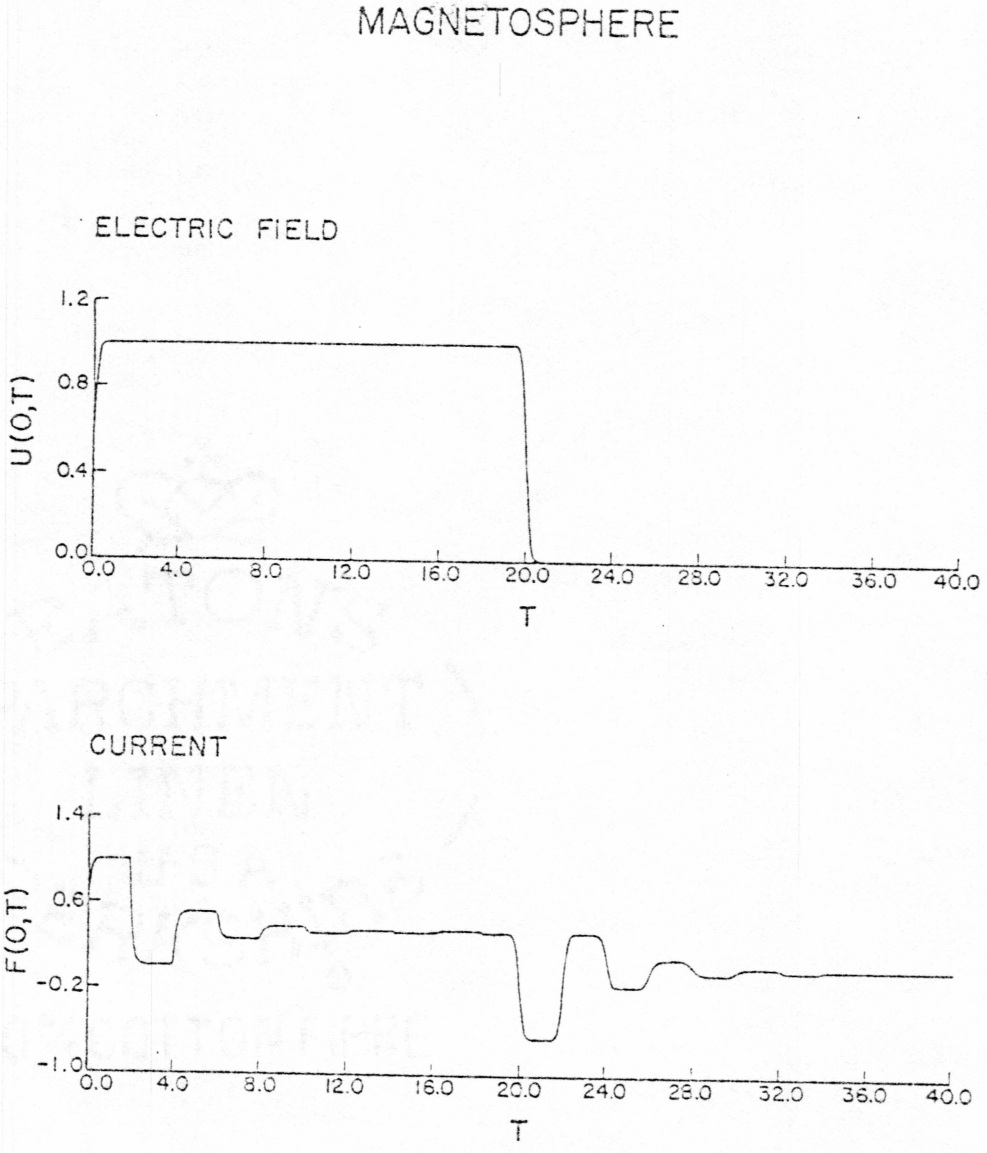

Fig. (3.5a) Plot of magnetospheric electric field and current for an enhancement of the magnetospheric convection with a short rise time and a long duration. The abscissa is in units of travel times. The ordinate is normmalize to the maximum magnetospheric electric field.

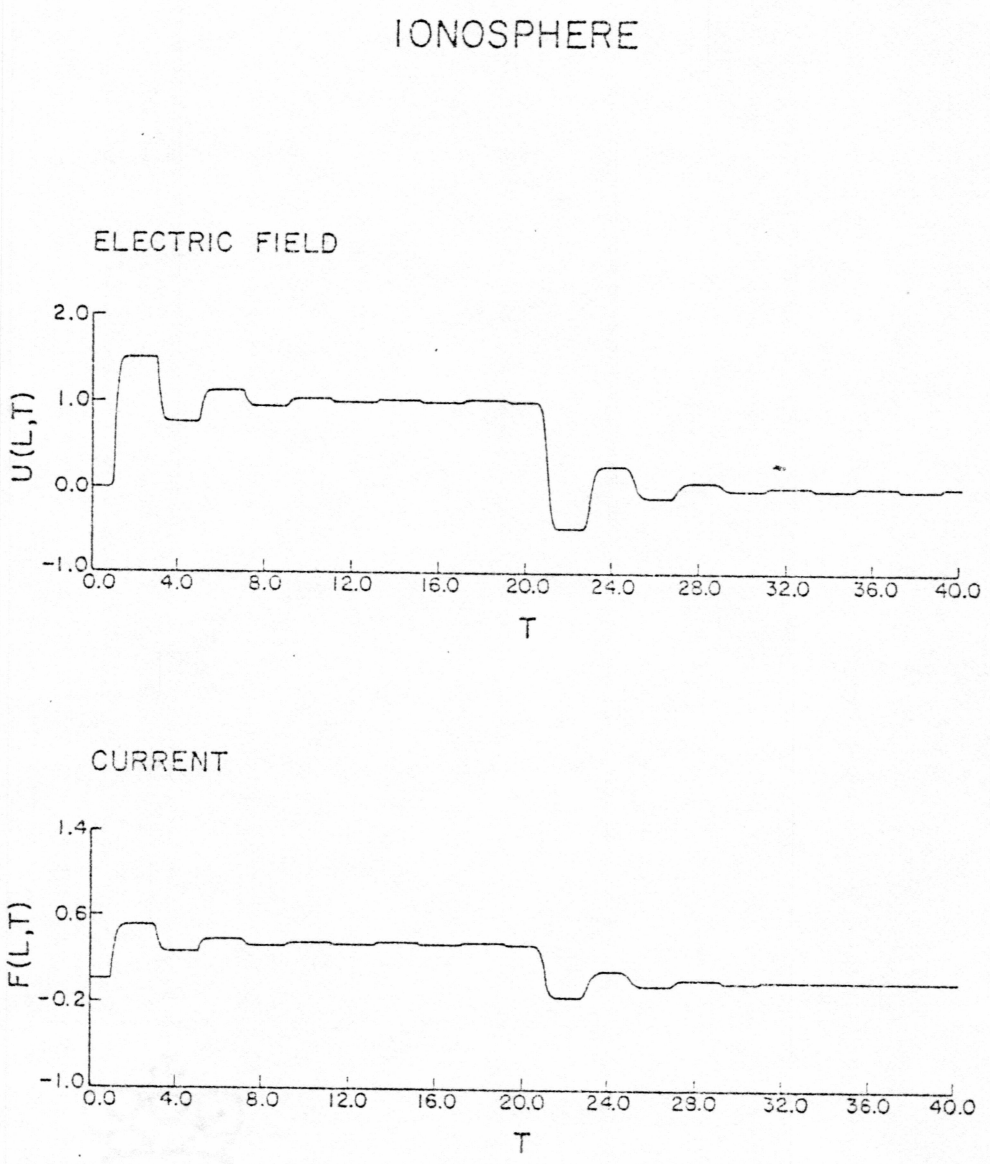

Fig. (3.5b) Plot of resultant ionospheric electric field and current for the enhancement of Fig. (3.5a).

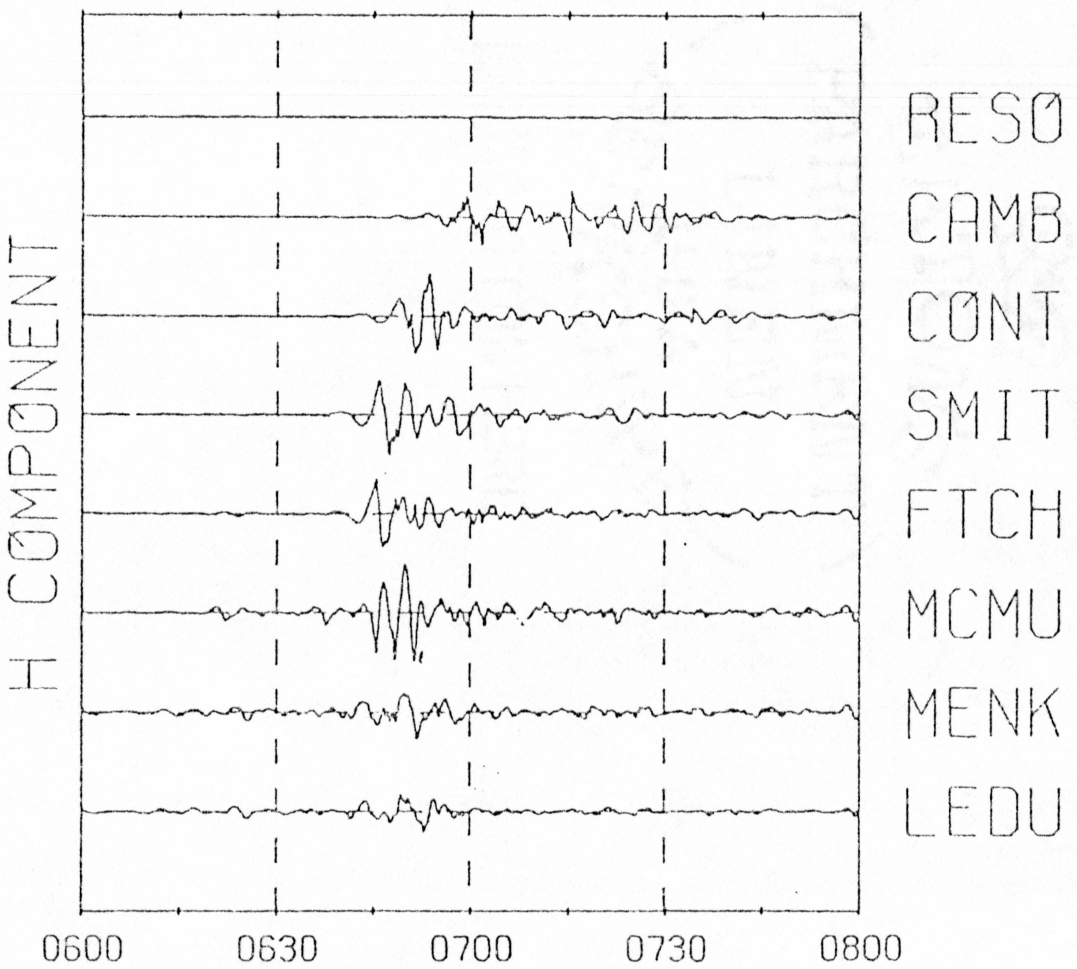

Fig. (3.6) Plot of horizonal magnetic perturbations recorded by the University of Alberta magnetometer chain for November 23, 1970.

transient response to a rapid rise in the magnetospheric enhancement of long duration will produce Pi 2 pulsations in the auroral ionosphere. The fundamental period of the oscillations in Fig. (3.5a) is $4T_o$. T_o can be estimated by assuming that electric field pulse and currents travel at the average Alfven speed of 2000 km/sec, and that the magnetospheric-ionospheric distance is about $10R_e$. The resultant period of oscillations is around 130 seconds, which is within the period range for Pi 2 pulsations.

3.5 Summary

In this chapter we have shown that the transient response of the magnetosphere-ionosphere coupling due to an enhancement of magnetospheric convection produces oscillations of ionospheric currents which can produce ground magnetic perturbations that have the characteristic form and period of Pi 2 pulsations. This was accomplished by solving numerically the one-dimensional wave equation which describes the physics of the magnetosphere-ionophere coupling. The results were compared to data collected by the University of Alberta.

IV CONCLUSION

We have seen that the slowing down of magnetospheric convection can be unstable to Alfven waves which can initiate broadband Pi 2 pulsations. For Pi 2 pulsations we also examined the transient response following an enhanced magnetospheric convection. The one-dimensional wave equation which describes the physics of the transient magnetospheric-ionospheric coupling was derived and solved numerically by the Lax-Wendroff method.

The computations indicate that a rapid increase in magnetospheric convection with a long duration can produce a damped oscillatory wave form in the ionospheric electric field and current. It was proposed that the oscillating current will produce a magnetic disturbance on the ground which will have the same general form as the ionospheric current. These magnetic disturbances could be considered Pi 2 pulsations since their general waveform and period were like that of observed Pi 2 pulsations. The period of oscillation is estimated to be around 130 seconds, within the range of Pi 2 pulsations. The computed waveforms are in qualitative agreement with those obtained from ground-based measurements and support the hypothesis of coupling between the magnetosphere and ionosphere for Pi 2 generation.

REFERENCES

Akasofu, S.-I., and S. Chapman, Solar Terrestrial Physics, Oxford University Press, Oxford, 1972.

Alfven, H., and C. Falthammer, Cosmical Electrodynamics, 2nd edition,Oxford University Press, London, 1963.

Angenheister, G., Uber die Fortpflanzungsgeschwindigkeit magneticher Storungen und Pulsationen, Bericht uber die erdmagnetischen Schnellregistrierungen in Apia (Samoa), Batavia, Cheltenhan und Tsingtau in September 1911, in Gottingen Nach Ges. Wiss., 568, 1912.

Atkinson, G., Auroral arcs: Results of the interaction of a dynamic magnetosphere with the ionosphere, J. Geophys. Res., 75, 4746, 1970.

Campbell, W. H., Geomagnetic pulsations, in Physics of Geomagnetic Phenomena, edited by S. Matsushita and W. H. Campbell, Academic Press, New York, 1967.

Chang, R. P. H., and L. J. Lanzerotti, On the generation of magnetohydrodynamic waves at the onset of a substorm, Geophys. Res. Lett., 2, 489, 1975.

Coroniti, F. V., and C. F. Kennel, Auroral micropulsation instability, J. Geophys. Res., 75, 1863, 1970.

Crawford, F. S., Waves, Berkeley Physics Course, vol. 1, McGraw-Hill, New York, 1968.

Gendrin, R., Substorm aspects of magnetic pulsations, Space Sci. Rev., 4, 54, 1970.

Goertz, C. K., and R. W. Boswell, Magnetosphere-ionosphere coupling, J. Geophys. Res., 84, 7739, 1979.

Heacock, R. R., Two subtypes of type Pi micropulsations, J. Geophys. Res., 72, 3905, 1967.

Heacock, R. R., and J. K. Chao, Type Pi2 magnetic field pulsastions at very high latitudes and their relation to plasma convection in the magnetosphere, J. Geophys. Res., 85, 1203, 1908.

Heacock, R. R., and R. D. Hunsucker, Type Pi2 magnetic field pulsations, Space Sci. Rev., 28, 191, 1981.

Heelis, R. A., and W. B. Hanson, High-latitude ion convection in the nighttime F region, J. Geophys. Res., 85, 1995, 1980.

Holzer, T. E., and T. Sato, Quiet auroral arcs and electrodynamic coupling between the ionosphere and the magnetosphere, 2, J. Geophys. Res., 78, 7330,1973.

Hones, W., E. Jr., S. J. Bame, and J. R. Asbridge, Proton flow measurements in the magnetotail plasma sheet made with IMP 6, J. Geophys. Res., 81, 227, 1976.

Jacobs, J. A., Geomagnetic Pulsations, Physics and Chemistry in Space, vol. 1, Springer, New York, 1970.

Jacobs, J. A., Y. Kato, S. Matsushita, and V. A. Troitskaya, Classification of geomagnetic micropulsations, J. Geophys. Res., 69, 180, 1964.

Johnson, W. C., Transmission Lines and Networks, McGraw-Hill, New York, 1950.

Kalikhman, L. E., Elements of Magnetogasdynamics, p. 79, Saunders Co., Philadelphia, 1967.

Kan, J. R., and R. R. Heacock, Generation of irregular (Type PiC) pulsations in the plasma sheet during substorms, J. Geophys. Res., 81, 2371, 1976.

Kan, J., R., and Lee, L. C., Theory of imperfect magnetosphere-ionosphere coupling, Geophys. Res. Lett., 7, 633, 1980.

Kan, J. R., L. C. Lee, Y. T. Chiu, and D. U. Longenecker, Generation of Alfven waves by deceleration of magnetospheric convection and broadband Pi pulsations, J. Geophys. Res., 87, 3511, 1982.

Kan, J. R., D. U. Longenecker, and J. V. Olson, A transient responce model of Pi2 pulsations, J. Geophys. Res., 87, 7483, 1982.

Krall, N. A., Drift waves, in Advances in Plasma Physics, vol. 1, edited by W. B. Thompson and A. Simon, Interscience, New York, 1968.

Krall, K. A., and A. W. Trivelpiece, Principles of Plasma Physics, McGraw-Hill, New York, 1973.

Lin, C. C., and L. J. Cahill, Pi 2 pulsations in the magnetosphere, Planet. Space Sci., 23, 693, 1975.

Mallinckrodt, A. J., and C. W. Carlson, Relations between transverse electric fields and field-aligned currents, J. Geophys. Res., 83, 1426, 1978.

Maltsev, Yu. P., S. V. Leontyev, and W. B. Lyatsky, Pi2 pulsations as a

result of evolution of an Alfven impulse originating in the ionosphere during a brightening of aurora, Planet. Space Sci., 22, 1519, 1974.

Maltsev, Yu. P., W. B. Lyatsky, and A. M. Lyatskaya, Currents over the auroral arc, Planet. Space Sci., 25, 53, 1977.

McPherron, R. L., and P. J. Coleman, Satellite observations of band limited micropulsations during a magnetospheric substorm, J. Geophys. Res., 76, 3010, 1971.

Miura, A., and T. Sato, Numerical simulation of global formation of auroral arcs, J. Geophys. Res., 85, 73, 1980.

Ogawa, T., and T. Sato, New mechanism of auroral arcs, Planet. Space Sci., 19, 1393, 1971.

Newton, R. S., D. J. Southwood, and W. J. Hughes, Damping of geomagnetic pulsations by the ionosphere, Planet. Space Sci., 26, 201, 1978.

Nishida, A., Possible origin of transient dusk to dawn electric field in the nightside magnetosphere, J. Geophys. Res., 84, 3409, 1979.

Nishida, A., and E. W. Hones, Associations of plasma sheet thinning with neutral line formation in the magnetotail., J. Geophys. Res., 79, 533,1974.

Olson, J. V., and G. Rostoker, Pi2 pulsations and the auroral electrojet, Planet. Space Sci., 23, 1129, 1975.

Olson, J. V., and G. Rostoker, Latitude variation of the spectral components of auroral zone Pi2, Planet. Space Sci., 25, 663, 1977.

Pashin, A. B., K. H. Glassmeier, W. Baumjohann, O. M. Raspopov, A. G. Yahnin, H. J. Opgenoorth, and R. J. Pellinen, Pi2 magnetic pulsations, auroral break-ups, and the substorm current wedge: a case study, J. Geophys., 51, 223, 1982.

Potter, D., Computational Physics, John Wiley and Sons, London, 1973.

Rostoker, G., The polarization characteristics of Pi-2 microplusations and their relation to the determination of possible source mechanisms for the production of nighttime impulsive micropulsation activity, Canadian J. Phys., 45, 1319, 1967.

Rostoker, G., and R. Bostrom, A mechanism for driving the gross Birkeland current configuration in the auroral oval, J. Geophys. Res., 81, 235,1976.

Rostoker, G., and H. -L. Lam, A generation mechanism for Pc5 micropulsation activity at the polar cusp, J. Geophys. Res., 77, 4700, 1972.

Rostoker, G., and J. V. Olson, Pi2 micropulsations as indicators of substorm onsets and intensifications, J. Geomag. Geoelec., 30, 135, 1978.

Rostoker, G., and J. C. Samson, Polarization characteristics of Pi2 pulsations and implications for their source mechanisms: location of source regions with respect to the auroral electrojets, Planet. Space Sci., 29, 225, 1981.

Sakurai, T., Substorm associated Pi2 magnetic pulsations, in Magnetospheric Dynamics, Proceedings of 1980 ISAS symposium, Univ. of Tokyo, Tokyo, 1981.

Saito, T., Geomagnetic pulsations, Space Sci. Rev., 10, 319,1969.

Saito, T., T. Sakurai, and Y. Koyama, Mechanisms of association between Pi2 pulsation and magnetospheric substorm, J. Atmos. and Terr. Phys., 38, 1265, 1976.

Sato, T., A theory of quiet auroral arcs, J. Geophys. Res., 83, 1042,1978.

Sato, T., and T. E. Holzer, Quiet auroral arcs and the electrodynamic coupling between the ionosphere and the magnetosphere, 1, J. Geophys. Res., 78, 7314, 1973.

Sonnerup, B. U. O., Theoty of the low-latitude boundary layer, J. Geophys. Res., 85, 2017, 1980.

Southwood, J. D., and W. F. Stuart, Pulsations at the substorm onset, in Dynamics of the Magnetosphere, edited by S. -I. Afasofu, D. Reidel Publ. Co., London, 1980.

Stewart, B., On the great magnetic disturbance which extended from August 28 to September 7, 1859, as recorded by photography at the Kew Observatory, Phil. Trans. Roy. Soc. London, 425, 1861.

Stuart, W. F., A special feature of impulsive pulsations (Pi2), J. Atmos. and Terr. Phys., 34, 829, 1972.

Stuart, W. F., A mechanism of selective enhancement of Pi2s by the plasmasphere, J. Atmos. and Terr. Phys., 36, 851, 1974.

Yumoto, K., T. Sato, A. Eitoku, and Y. Kamide, A statistical study of low-latitude substorms, in Magnetospheric Dynamics, Proceedings of

1980 ISAS symposium, Univ. of Tokyo, Tokyo, 1981.

A P P E N D I X

THE MHD APPROXIMATION

To justify the use of the MHD equations, the MHD approximation (Krall and Trivalpiece, 1973 p. 97), must hold:

$$(r_L/L)^2 \ll \frac{1}{T\omega_{ci}} \ll 1, \qquad (A.1)$$

where r_L is the Larmor radius of the ions, L is the scale length, T is the characteristic time and ω_{ci} is the ion cyclotron frequency. The Larmor radius is given by

$$r_L = \frac{mv_\perp}{eB}, \qquad (A.2)$$

where m,v and e are the ion mass, parallel velocity and charge respectively. B is the average magnetic induction along the field line. To test the inequalities in (A.1) the magnetic field is approximated by a dipole field. The magnitude of the field is given by

$$B = \frac{a}{r^3}\sqrt{(1+3\sin^2\lambda)}, \qquad (A.3)$$

where a is the magnetic moment of the geomagnetic field, r is the distance from the center of the earth and λ is the colatitude. The magnetic moment has a value of 8.1×10^{25} tesla-m^3 (Alfven and Falthammer, 1963). The average magnetic field value along the field

line can be found by applying (A.3). The field line intersects the earth at r = 1 Re and l = 70°. This field line will intersect the geomagnetic equator at about 10 Re, thus the scale length of the magnetosphere-ionosphere system is 10 Re. By taking samples of the magnetic field at 1 Re intervals the average magnetic field is found to be on the order of 10^{-6} tesla. Using this result in eq. (A.2) along with the scale length, the left hand side of (A.1) can be calculated

$$(r_L/L)^2 \approx 10^{-10}. \qquad (A.4)$$

The ion cyclotron frequency is given by

$$\omega_{ci} = \frac{eB}{m},$$

where e and m are the ion charge and mass respectively. Again B is the average magnetic field. Assuming a time scale of about one minute, the middle part of (A.1) is

$$1/T\omega_{ci} \approx 10^{-5}. \qquad (A.5)$$

Equations (A.4) and (A.5) satisfy (A.1), therefore the MHD equations can be applied to this system.